JOURNAL OF PETROLOGY | VOLUME 45 | NUMBER 7 | PAGES 1393–1412 | 2004 | DOI: 10.1093/petrology/egh017

Metapelites of the Kanskiy Granulite Complex (Eastern Siberia): Kinked *P–T* Paths and Geodynamic Model

TARAS V. GERYA[1,2]* AND WALTER V. MARESCH[2]

[1]INSTITUTE OF EXPERIMENTAL MINERALOGY, RUSSIAN ACADEMY OF SCIENCES, CHERNOGOLOVKA, MOSCOW DISTRICT, 142432, RUSSIA

[2]INSTITUT FÜR GEOLOGIE, MINERALOGIE UND GEOPHYSIK, RUHR-UNIVERSITÄT BOCHUM, UNIVERSITÄTSTRASSE 150, 44780 BOCHUM, GERMANY

RECEIVED NOVEMBER 15, 2002; ACCEPTED JANUARY 1, 2003

The Southern Yenisey Range (Eastern Siberia) consists of the granulite-facies Kanskiy complex bordered by the lower-grade Yeniseyskiy and Yukseevskiy complexes. Samples of metapelite of the Kanskiy complex typically show characteristic garnet-forming reaction textures and near-isobaric cooling P–T *paths. An important new result of this study concerns the difference in shape of the* P–T *paths from different parts of the Kanskiy granulite complex: metapelites collected ~8 km from the boundary with the Yeniseyskiy complex followed a linear path with* $dP/dT \approx 0{\cdot}006$ *kbar/°C; metapelites collected ~3 km from this boundary reveal a kinked* P–T *path with an interval of burial cooling (*$dP/dT \approx -0{\cdot}006$ *kbar/°C). The difference in the shape of the* P–T *paths is supported by the chemical zoning of garnet studied in the second group of samples. A mechanism of buoyant exhumation of granulite is suggested by comparison with the results of numerical modelling, which indicate that such a diversity of* P–T *paths may result from a transient disturbance of the thermal structure by rapid differential movement of material from different crustal levels. To arrive at a correct tectonic interpretation, the whole assemblage of interrelated* P–T *paths of metamorphic rocks collected from different localities within the same complex must be studied.*

KEY WORDS: *crustal diapirism; exhumation; granulites; numerical modelling;* P–T *path*

INTRODUCTION

This paper addresses the petrology and *P–T* history of metapelitic gneisses of the Kanskiy granulite complex in the Southern Yenisey Range (Eastern Siberia). Numerical modelling of these data allows the exhumation history of this high-grade terrain to be constrained.

Recent studies of Precambrian high-grade granulite complexes and adjacent lower-grade cratonic granite–greenstone terrains in Southern Africa and Russia suggest that both low- and high-grade metamorphic rocks from these areas record evidence for the metamorphic and tectonic events leading to the thrusting of granulites onto the adjacent granite–greenstone terrains (e.g. Perchuk, 1989; Van Reenen *et al.*, 1990; Roering *et al.*, 1992*a*, 1992*b*; Mints *et al.*, 1996; Perchuk *et al.*, 1996, 1999, 2000*a*, 2000*b*; Pozhilenko *et al.*, 1997; Perchuk & Krotov, 1998). In Southern Africa (the Southern Marginal Zone of the Limpopo complex) and in the Kola Peninsula (the Lapland complex) regional, crustal-scale shear zones separate the granulite terrains from the lower-grade granite–greenstone terrains. The emplacement of relatively hot, ductile granulites onto relatively cold, brittle cratonic successions caused heat transfer from the exhuming granulites to the underlying wall rocks, resulting in the development of dynamic polythermal–polybaric metamorphic zoning (Roering *et al.*, 1992*a*; Perchuk *et al.*, 1996; Perchuk & Krotov, 1998).

Published data (e.g. Kusnetsov, 1941, 1988; Kovrigina, 1973, 1977; Nozkhin, 1983, 1985; Gerya *et al.*, 1986; Perchuk *et al.*, 1989; Dacenko, 1995) suggest that the Southern Yenisey Range of Eastern Siberia is composed of metamorphic complexes of different metamorphic grade separated by regional thrusts (Fig. 1). The degree of metamorphism generally increases across the thrust system from greenschist- and epidote–amphibolite-facies conditions (the Yukseevskiy complex) through amphibolite-facies (the Yeniseyskiy complex) to granulite-facies

*Corresponding author. Present address: Institut für Geologie, Mineralogie und Geophysik, Ruhr-Universität Bochum, Universitätstrasse 150, 44780 Bochum, Germany. Telephone: 49-234-3223518. Fax: 49-234-3214433. E-mail: taras.gerya@ruhr-uni-bochum.de

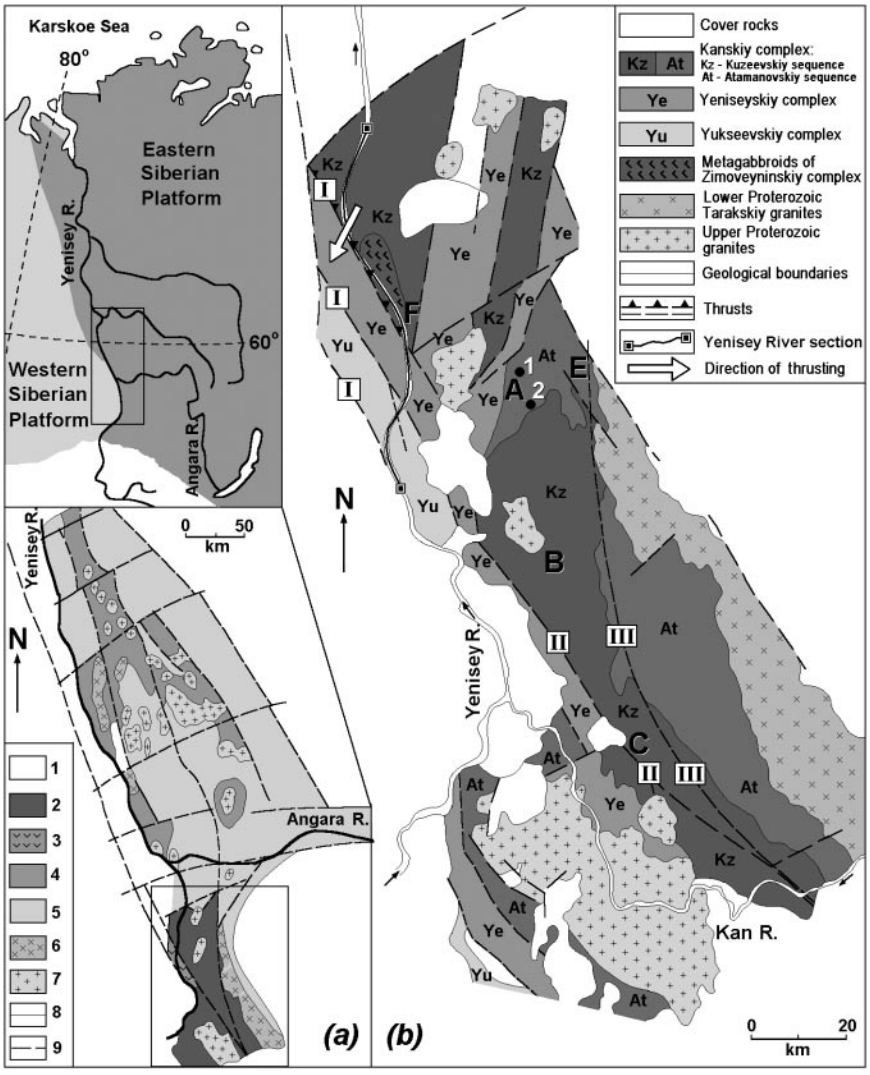

Fig. 1. Regional position (a) and geological structure (b) of the Southern Yenisey Range, Eastern Siberia. (a) Main geological units of the Yenisey Range. 1, cover rocks; 2–4, Pre-Riphean metamorphic complexes: 2, Kanskiy and Yeniseyskiy granulitic–gneissic complexes, amphibolite- to granulite-facies metamorphism (>1900 Ma); 3, Yukseevskiy greenstone complex, greenschists to epidote–amphibolite-facies metamorphism (>1900 Ma); 4, Teyskiy complex (gneisses, carbonate rocks, quartzites, micaceous schists, metabasites), greenschist- to amphibolite-facies metamorphism (>1650 Ma); 5, Riphean volcanic and sedimentary complexes; 6, Lower Proterozoic granitoids; 7, Upper Proterozoic granitoids; 8, geological boundaries; 9, thrusts. (b) Geological map of the Southern Yenisey Range. Major regional thrust systems: I, Pri-Yeniseyskiy; II, Kansko-Posolnenskiy; III, Kansko-Shilkinskiy. Circles with numbers show the location of samples listed in Table 1: 1—A257, A-256, A-258, A-260, A-269, A-271, A-275; 2—A-538, A-643, A-720. A, B, C, E and F are specific localities referred to in the text.

conditions (the Kanskiy complex) (e.g. Kusnetsov, 1941, 1988; Gerya *et al.*, 1986; Perchuk *et al.*, 1989). Recent combined structural and petrological studies (Smit *et al.*, 2000) suggest that all three complexes are characterized by a uniform D_2 shear pattern that was formed during the exhumation of the Kanskiy complex.

Smit *et al.* (2000) suggested that both the tectono-metamorphic pattern and the evolution of the metamorphic complexes of the Southern Yenisey Range are very similar to those described for the *c.* 2600 Ma Limpopo complex of Southern Africa and the *c.* 1900 Ma Lapland complex of the Kola Peninsula. Similar geodynamic processes therefore appear to be responsible for the formation of these high-grade terrains. Similarities in the reaction textures of granulites in all three metamorphic terrains have also been recognized (Perchuk *et al.*, 2000*b*). However, in both the Limpopo and Lapland complexes, metapelitic granulites show characteristic garnet-forming reaction textures that can be related to a distinctively kinked retrograde P–T path (Fig. 2) with an intermediate near-isobaric cooling interval (dP/dT = 0·007–0·008 kbar/°C, Perchuk *et al.*, 2000*b*; Smit *et al.*, 2001). Such P–T paths have so far not been described for the Kanskiy granulite complex (Perchuk *et al.*, 1989).

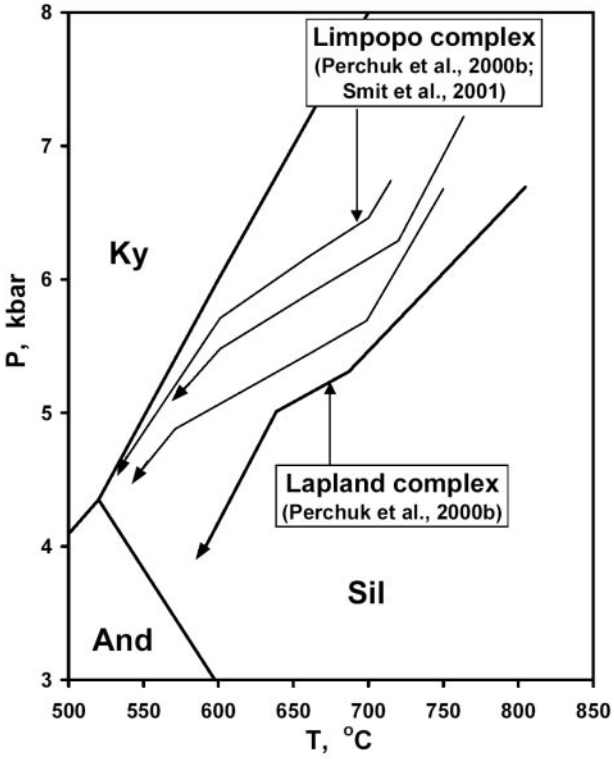

Fig. 2. Typical examples of kinked *P–T* paths in metapelites of the Limpopo and the Lapland granulite complexes, as inferred from mineral zoning and reaction textures (Perchuk *et al.*, 2000*b*; Smit *et al.*, 2001).

In this paper we present the first evidence that kinked retrograde *P–T* paths are also found in metapelitic granulites sampled close (~3 km) to the border of the Kanskiy granulite complex, allowing us to discuss the geodynamic significance of this phenomenon.

GEOLOGICAL SETTING

The Yenisey Range is situated in the major Baikalide belt that subdivides Siberia into Western and Eastern Platforms (Fig. 1). The Baikalide belt occurs as a semi-circular rim around the Eastern Siberian Platform that, among other geological features, also hosts the Yenisey Range (Fig. 1a). The Yenisey Range is about 700 km in length and 150 km wide and consists of metamorphic, magmatic and sedimentary complexes of Archaean to Cenozoic age (Fig. 1a). The Southern Yenisey Range (Fig. 1b) constitutes a Precambrian metamorphic terrain with an exposed outcrop length of about 200 km and a width of 50–70 km. The regional structural framework of the Southern Yenisey Range has been traditionally interpreted as a system of north–south- to NW–SE-oriented crustal blocks (e.g. Kovrigina, 1973, 1977; Dacenko, 1995). On the basis of metamorphic, petrological and geochemical evidence, a subdivision into the Kanskiy, Yeniseyskiy and Yukseevskiy complexes has been recommended (Kusnetsov, 1941, 1988; Nozkhin, 1983, 1985; Gerya *et al.*, 1986; Perchuk *et al.*, 1989). These blocks are characterized internally by large-scale (100–800 m) isoclinal folds with axial planes dipping to the NE, well-developed lineations and a regional schistosity. Thrusts in the area follow the general structural trend of the Range and three major regional thrust systems are distinguished from west to east (Fig. 1b): the Pri-Yeniseyskiy, Kansko-Posolnenskiy and Kansko-Shilkinskiy thrusts (Kovrigina, 1973). Their orientation changes from NW–SE in the south to north–south in the north, following the contours of the Siberian Craton. The thrust systems, which dip at 50–70°E to the NE, with a general vergence towards the west, are composed of up to 4 km wide zones of mylonitization and are characterized by the presence of magmatic complexes and hydrothermal ore deposits. This uniform structural pattern across the Southern Yenisey Range has been traditionally attributed to folding during the systematic accretion of the Kanskiy, Yeniseyskiy and Yukseevskiy metamorphic complexes onto the western boundary of the Eastern Siberian Craton (e.g. Dacenko, 1995). Recently, however, Smit *et al.* (2000) studied the structural–metamorphic evolution of the Kanskiy, Yeniseyskiy and Yukseevskiy complexes of the Southern Yenisey Range along the Yenisey River section (Fig. 1). Three deformational events were recognized in each of the three complexes: a D_1 fabric-forming event, a D_2 shear and folding event, and a D_3 shear event. Thrust kinematics across the Southern Yenisey Range suggest that during the D_2 event the Kanskiy complex was thrust along a regional ductile shear zone onto the lower-grade complexes. This resulted in shearing and folding as well as the development of a dynamic metamorphic zonation.

The major stage of granulite-facies metamorphism in the Kanskiy complex was dated at 1800–2000 Ma, based on the zircon studies of Nozkhin *et al.* (1989) and Bibikova *et al.* (1993). This age correlates well with the 1900 ± 100 Ma emplacement age of the Tarakskiy granites (Gerling & Artemov, 1964; Volobuev *et al.*, 1976). An early thermal event is indicated for the period 2650 ± 50 Ma (Nozkhin *et al.*, 1989; Bibikova *et al.*, 1993), but the age of the protolith must exceed 2700 Ma. The major stage of epidote–amphibolite- to amphibolite-facies metamorphism in the Yeniseyskiy complex (1850 ± 150 Ma, Nozkhin *et al.*, 1989; 1900–1860 Ma, Bibikova *et al.*, 1993) correlates with the main granulite-facies event in the Kanskiy complex. A wide range of zircon ages have been determined for the rocks of the Yukseevskiy complex (Nozkhin *et al.*, 1989; Nozkhin, 1997): 2750 Ma, 1900 Ma, 1450 Ma, 1050 Ma, 870 Ma and 600 Ma. Nozkhin *et al.* (1989) interpreted the 2750 Ma age as the time of formation of the volcano-sedimentary protolith of

the Yukseevskiy complex and the 1450 Ma stage as the time of formation of the regional sub-meridional tectonic structure (Fig. 1a) of the entire Yenisey Range (Nozkhin *et al.*, 1989). The three youngest ages correlate with the intrusion of Upper Proterozoic granites into the Kanskiy complex (Volobuev *et al.*, 1976, 1980; Dacenko, 1984; Nozkhin *et al.*, 1989).

Although the geochronology of the area is thus based on a very limited database, it does indicate that important metamorphic events occurred during the period 1800–2000 Ma in all three complexes of the Southern Yenisey Range. This period corresponds to the peak of the thermal activity in the area and to the formation of the Tarakskiy granitoid batholith during the final stages of granulite-facies metamorphism. According to the interpretation of Smit *et al.* (2000), the major D_2 stage of the metamorphism in all three complexes in the period 2000–1800 Ma corresponds to deformation and heat transfer caused by the exhumation of the Kanskiy complex. The D_3 mylonitization event, on the other hand, was related to the formation of large-scale mylonitic shear zones (Fig. 1a and b) that occur across the entire Yenisey Range, dated at 1450 Ma by Nozkhin *et al.* (1989).

GEOLOGY OF THE KANSKIY GRANULITE COMPLEX

The Kanskiy granulite complex is subdivided into a lower Kuseevskiy and an upper Atamanovskiy sequence (Fig. 1b). The Kuseevskiy sequence is mainly composed of garnet–plagioclase, garnet–orthopyroxene–plagioclase and orthopyroxene–plagioclase gneisses and granulites, orthopyroxene–spinel–plagioclase ± garnet metabasites, aluminous metapelites with garnet, cordierite, sillimanite, spinel and orthopyroxene, as well as some charnockites and enderbites. The sequence also contains several metagabbro massifs of the Zimoveyninskiy complex (Fig. 1b). The assemblage quartz + orthopyroxene + sillimanite that characterizes peak (T ~900°C and P ~8 kbar) metamorphic conditions is found in some metapelites of the sequence (Perchuk *et al.*, 1989). Maximum P–T conditions recorded in garnet–cordierite–sillimanite–quartz metapelites correspond to 795°C and 6·1 kbar (Perchuk *et al.*, 1989).

The Atamanovskiy sequence consists of aluminous garnet–biotite, garnet–cordierite–biotite, garnet–cordierite–sillimanite–spinel–two-feldspar metapelites, orthopyroxene–garnet–biotite, orthopyroxene–biotite–cordierite and orthopyroxene–plagioclase gneisses and rare orthopyroxene–spinel–plagioclase metabasites. The assemblage quartz + orthopyroxene + sillimanite is not found in metapelites of the sequence and the maximum P–T conditions recorded in garnet–cordierite–sillimanite–quartz metapelites are 716°C and 4·5 kbar (Perchuk *et al.*, 1989). In the NE part of the area near the Tarakskiy pluton (locality E in Fig. 1b) some metapelites of the Atamanovskiy sequence contain andalusite (Serenko, 1969; Perchuk *et al.*, 1989). The intensively migmatized northeastern portion of the sequence demonstrates a gradual transition into granites of the Tarakskiy pluton (Dacenko, 1984).

Metapelites from both sequences of the Kanskiy complex show near-isobaric cooling reaction textures such as replacement of cordierite by garnet, sillimanite and quartz (Perchuk *et al.*, 1989). These textures are more characteristic for metapelites taken from areas farthest from the Tarakskiy pluton and closest to the contacts between the Kanskiy and the Yeniseyskiy complexes (localities A, B and C in Fig. 1b) (Perchuk *et al.*, 1989). In the western part of the area close to the Yenisey river this contact is also marked by the appearance of orthopyroxene + sillimanite in metapelites (e.g. localities A and B in Fig. 1b) and orthopyroxene + spinel + garnet + plagioclase in metabasites (e.g. localities A, B and F in Fig. 1b) of the Kuseevskiy sequence (Serenko, 1969; Perchuk *et al.*, 1989).

Despite their high-grade character, the major rock types of the Kanskiy complex are geochemically very similar to typical Archaean granite–greenstone complexes (Nozkhin & Turkina, 1993): the garnet–orthopyroxene–biotite gneisses are analogous to volcanic rocks of andesitic and dacitic composition, whereas the aluminous gneisses are similar to pelitic rocks. The orthopyroxene–spinel–plagioclase metabasites demonstrate characteristics of tholeiitic basalts. The average chemical composition of the Kanskiy complex corresponds to granodiorite (Nozkhin & Turkina, 1993). An increase in the relative amount of mafic rocks in a northwesterly direction within the Kanskiy complex was described by Nozkhin & Turkina (1993). The most significant amount of granulite-grade metabasic rock is concentrated along the Yenisey River, including the 1·5 km × 25 km layered Zimoveyninskiy metagabbro massif (Fig. 1b).

MINERALOGY AND PETROLOGY OF STUDIED SAMPLES

For petrological study we selected 11 samples of metapelite containing the assemblage garnet + cordierite + sillimanite + quartz + K-feldspar + plagioclase + biotite collected from the rocks of the Atamanovskiy sequence from two localities at different distances (~3 km and ~8 km, see Fig. 1) from the boundary with the Yeniseyskiy complex. Mineral assemblages and bulk chemical compositions of these samples are listed in Tables 1 and 2, respectively. Microprobe analyses of coexisting minerals from these samples were carried out using the CamScan scanning electron microscope

Table 1: Mineral assemblages of metapelites studied

Sample	Locality (see Fig. 1)	Mineral assemblage
A-256	1	Qtz + Pl + Kfs + Grt + Bt + Crd + Spl + Sil + Ilm + Mag
A-257	1	Qtz + Pl + Kfs + Grt + Bt + Crd + Spl + Sil + Ilm + Mag
A-258	1	Qtz + Pl + Kfs + Grt + Bt + Crd + Spl + Sil + Ilm + Mag
A-260	1	Qtz + Pl + Kfs + Grt + Bt + Crd + Spl + Sil + Ilm + Mag
A-269	1	Qtz + Pl + Kfs + Grt + Bt + Crd + Sil + Ilm + Mag
A-271	1	Qtz + Pl + Kfs + Grt + Bt + Crd + Spl + Sil + Ilm + Mag
A-274	1	Qtz + Pl + Kfs + Grt + Bt + Crd + Spl + Sil + Ilm + Mag
A-275	1	Qtz + Pl + Kfs + Grt + Bt + Crd + Spl + Sil + Ilm + Mag
A-538	2	Qtz + Pl + Kfs + Grt + Bt + Crd + Spl + Sil + Opx* + Ilm + Mag
A-643	2	Qtz + Pl + Kfs + Grt + Bt + Crd + Spl + Sil + Crn† + Ilm + Mag
A-720	2	Qtz + Pl + Kfs + Grt + Bt + Crd + Spl + Sil + Crn† + Ilm + Mag

*Orthopyroxene occurs in intergrowth with biotite and cordierite and does not coexist with sillimanite + quartz.
†Corundum occurs in intergrowth with spinel and magnetite and does not coexist with quartz.
All mineral abbreviations used in this paper are after Kretz (1983).

Table 2: Bulk chemical compositions of metapelites studied*

Sample:	A-256	A-257	A-258	A-260	A-269	A-271	A-274	A-275	A-538	A-643	A-720
SiO_2	53·35	72·28	60·72	66·79	65·04	74·15	61·89	62·50	56·64	51·49	53·52
TiO_2	0·93	0·70	0·99	0·78	0·61	0·74	0·94	0·95	0·88	1·22	0·96
Al_2O_3	19·63	13·07	19·44	16·95	16·43	12·01	18·93	18·10	21·61	24·50	22·09
Fe_2O_3	2·50	1·74	2·74	2·00	0·32	2·06	2·25	1·41	0·90	3·91	5·13
FeO	6·60	4·41	6·98	5·12	5·84	3·17	6·84	6·94	7·96	9·49	7·13
MnO	0·13	0·02	0·19	0·06	0·05	0·04	0·14	0·08	0·09	0·11	0·06
MgO	5·15	1·32	3·02	1·99	1·95	1·43	2·18	3·02	2·96	3·89	2·49
CaO	2·90	0·56	0·59	0·57	2·51	1·10	0·48	1·81	0·82	0·83	0·54
Na_2O	1·94	0·97	0·97	0·97	1·95	1·24	1·02	1·62	1·35	0·87	1·40
K_2O	4·87	4·15	3·24	3·96	4·49	3·33	4·20	2·47	6·27	3·38	5·70
P_2O_5	0·10	0·06	0·10	0·06	0·16	0·08	0·14	0·10	0·07	0·11	0·11
LOI	1·18	0·73	1·00	0·76	0·79	0·67	0·99	0·99	0·35	0·48	0·94
Total	99·28	100·01	99·98	100·01	100·14	100·02	100·00	99·99	99·90	100·28	100·07

*Chemical compositions are analysed using 'wet chemistry' method.

equipped with EDS Link AN10/85S at the Department of Petrology, Moscow State University, as well as the Cameca electron microprobe analyzer of the Institute of Experimental Mineralogy, Russian Academy of Sciences. Selected microprobe analyses of studied minerals are given in the Electronic Appendix to this paper, which may be downloaded from the *Journal of Petrology* website at http://www.petrology.oupjournals.org/.

The fabric of the metapelites is dominated by porphyroblasts of garnet and cordierite set in a matrix of sillimanite, quartz, K-feldspar, plagioclase and biotite (Figs 3 and 4). As will be shown below, these garnet and cordierite compositions reflect *P–T* conditions close to peak metamorphism and early stages of cooling. They will be referred to as Grt_1 and Crd_1 in the following discussion. Early generation Grt_1 is represented by large (3–10 mm) isometric poikiloblasts containing abundant quartz and biotite inclusions (Fig. 3a, c and d). First generation Crd_1 also forms large (1–3 mm) isometric, inclusion-rich poikiloblastic grains (Fig. 3b)

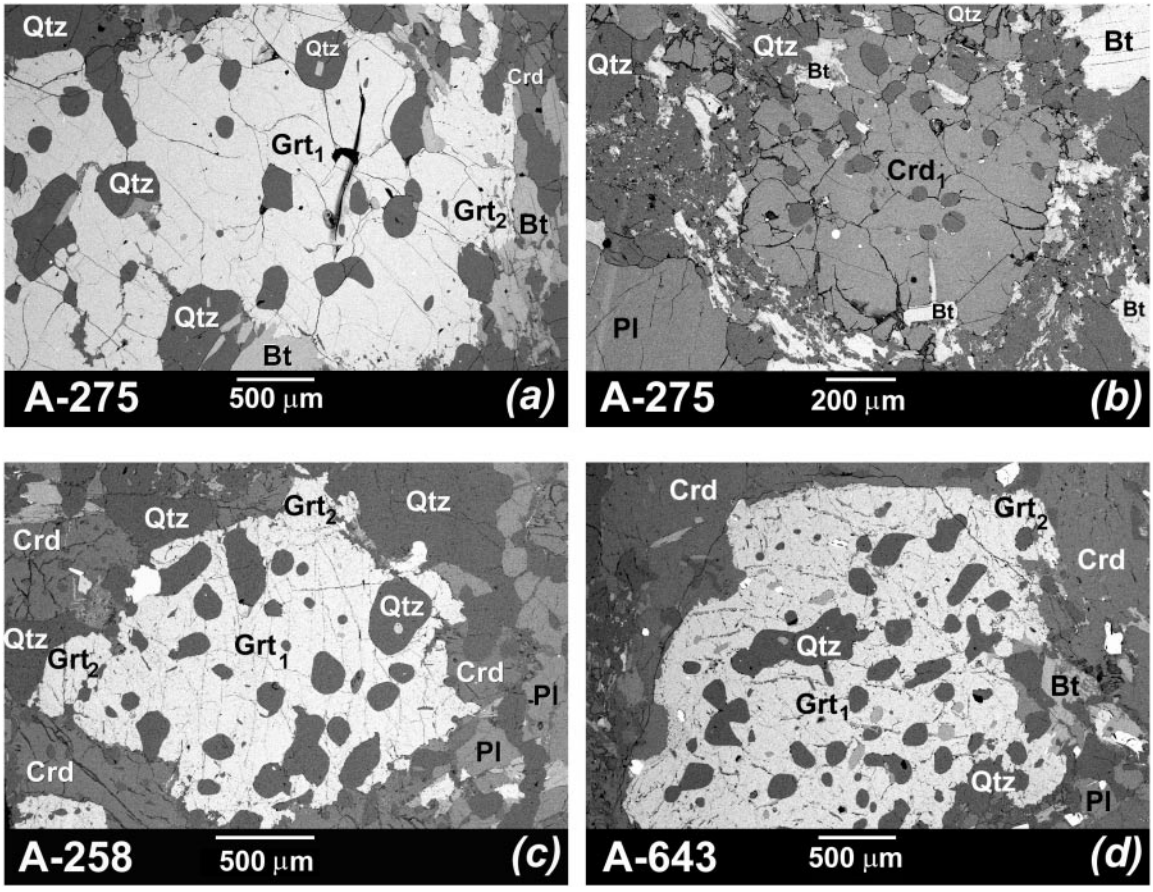

Fig. 3. Back-scattered electron images of early garnet (Grt_1) (a, c, d) and cordierite (Crd_1) (b) porphyroblasts in samples studied.

or aggregates. In both localities studied, Crd_1 contains conspicuous spinel + quartz symplectites (Fig. 4a and b) formed by decomposition of the cordierite according to the reaction

$$Crd_1 \rightarrow Spl + Qtz \quad (1)$$

presumably at some early stage of the high-temperature history of the rock.

A second, younger generation of garnet (Grt_2) is found in thin ($\leq$0·2 mm) garnet–sillimanite–quartz intergrowths formed at the contact between the early poikiloblastic garnet with early cordierite (Fig. 5). Small ($\leq$0·1 mm) idioblastic crystals of garnet are characteristic of this reaction texture (Fig. 6). The intergrowths can be interpreted as forming by decomposition of cordierite according to the reaction

$$Crd_1 \rightarrow Grt_2 + Sil + Qtz. \quad (2)$$

Similar intergrowths have been described from the Limpopo and the Lapland granulite-facies terrains (Perchuk *et al.*, 1996, 2000*b*; Smit *et al.*, 2001).

The designation Crd_2 is used here for non-porphyroblastic cordierite in medium- to fine-grained intergrowth with Grt_2, sillimanite, biotite, plagioclase and quartz (Figs 5 and 6). Because of the small grain size, these crystals have equilibrated with Grt_2 during the cooling history of the rock.

In sample A-538 (Table 1) specific reaction textures occur involving biotite and K-feldspar (Fig. 4c and d). In this sample, biotite grains and biotite–sillimanite intergrowths are commonly replaced by cordierite and orthopyroxene (Fig. 6c) without the formation of other potassium-bearing phases. This suggests dehydration reactions, with associated loss of the potassium component into the melt or metamorphic fluid, caused either by a temperature rise or a decrease in water activity. On the other hand, inclusions of quartz in early poikiloblastic garnet (Grt_1) are commonly surrounded by K-feldspar microveins (Fig. 4d). Similar reaction textures related to the charnockitization process have been described in granulites from several regions and reflect mobility of potassium in the presence of either metamorphic fluid or partial melt during granulite-facies metamorphism (e.g. Perchuk & Gerya, 1992, 1993; Perchuk *et al.*, 1994, 2000*c*; Newton, 1995).

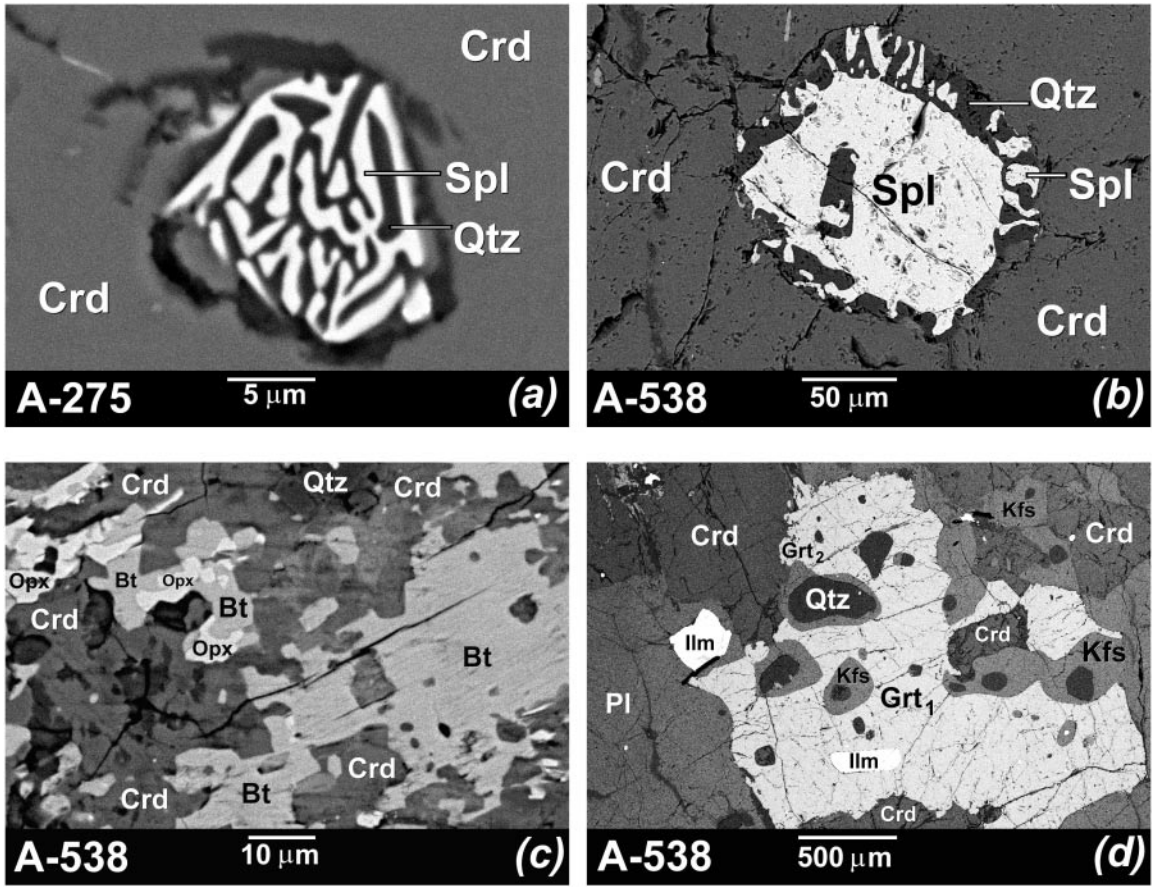

Fig. 4. Typical examples of reaction textures. (a, b) Replacement of cordierite by spinel + quartz intergrowths in samples A-275 (a) and A-538 (b). (c) Replacement of biotite by cordierite and orthopyroxene in sample A-538. (d) K-feldspar aureoles formed at the contact between garnet and quartz in sample A-538.

Figures 6–8 show typical zoning profiles of coexisting garnet and cordierite of different generations. It is seen that both Crd_1 and Crd_2 are characterized by a significant increase in Mg content from the core [$X_{Mg} = 0{\cdot}6$–$0{\cdot}7$, where $X_{Mg} = Mg/(Mg + Fe)$] toward the rim ($X_{Mg} = 0{\cdot}75$–$0{\cdot}8$), particularly in contact with garnet. Chemical zoning of garnet is different in samples from the two localities. Early poikiloblastic garnet (Grt_1) from sample A-275 collected close to the boundary of the Kanskiy complex in several cases demonstrates a notable decrease in Mg content from the core ($X_{Mg} = 0{\cdot}19$–$0{\cdot}21$) to the rim ($X_{Mg} = 0{\cdot}16$–$0{\cdot}17$, Fig. 7b), whereas similar garnet in samples A-538 and A-643 collected further away from this boundary is characterized by relatively constant Mg contents ($X_{Mg} = 0{\cdot}23$–$0{\cdot}25$, Fig. 8a and b). Second generation garnet (Grt_2) in all samples commonly shows an increase in Mg content ($X_{Mg} = 0{\cdot}23$–$0{\cdot}24$ in the core, $X_{Mg} = 0{\cdot}26$–$0{\cdot}31$ in the rim) toward the contact with cordierite. This is observed for both younger idioblastic Grt_2 grains (Fig. 6b and d) and in garnet + sillimanite + quartz intergrowths surrounding Grt_1 porphyroblasts (Figs 7a, b, and 8a, b), and is especially characteristic for samples collected close to the contact of the Kanskiy granulite complex with the Yeniseyskiy complex.

THERMOBAROMETRY AND *P–T* PATHS

Methods

Thermobarometry of granulites is recognized as a complex problem that cannot be solved only by the simple routine methods applicable to lower-grade metamorphic rocks (e.g. Frost & Chacko, 1989; Spear & Florence, 1992; Spear, 1993). Frost & Chacko (1989) concluded that special care must be taken to maximize the chance of correct retrieval of peak metamorphic conditions and accurate retrograde *P–T* paths for granulites. One of the most crucial criteria is the interpretation of reaction textures to test and corroborate the *P–T* trajectories obtained on the basis of thermobarometry alone (e.g. Frost & Chacko, 1989; Harley, 1989).

The approach and methods adopted here have been discussed and validated at length by Smit *et al.* (2001).

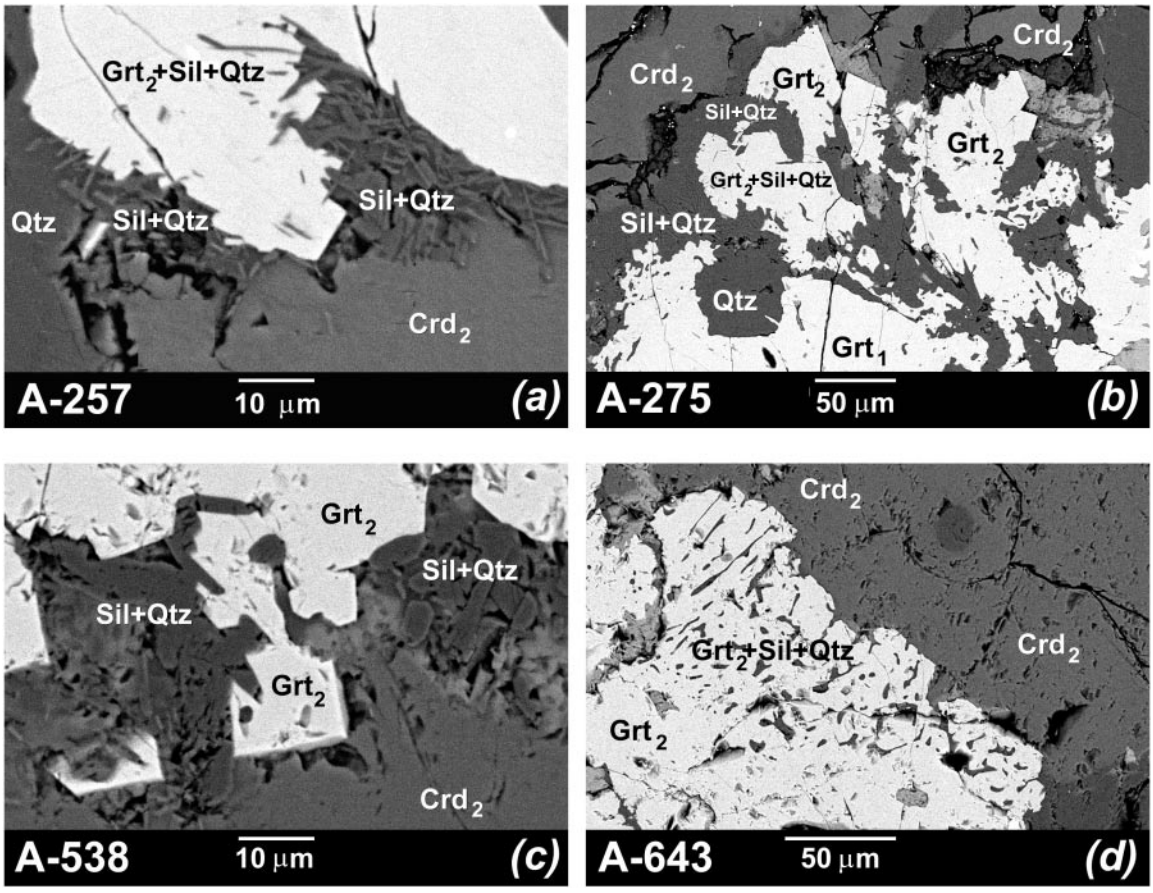

Fig. 5. Back-scattered electron images of later garnet (Grt_2) and garnet + sillimanite + quartz intergrowths replacing cordierite in samples studied.

Critical aspects are the assumption that the cores of large grains can remain unaffected by later diffusion, whereas the rims reflect re-equilibration. Because reaction (2) leads to armouring of garnet and cordierite by quartz–sillimanite intergrowths, late Fe, Mg exchange in these reaction zones is arrested and intermediate stages of the cooling trajectory can be monitored. In addition, the net transfer reactions implied by specific P–T trajectories must be corroborated by modal changes, i.e. reaction textures, in the rock.

Another important aspect is the corroboration of a P–T trajectory via the pattern of chemical zoning of the minerals involved in the net transfer and exchange reactions. Inferred changes in dP/dT along the P–T trajectory should be reflected in corresponding changes in the chemical zoning patterns of these minerals. This qualitative and relative test reflects discontinuities in trend vectors and does not depend directly on the absolute accuracy of individual P–T estimates defined by uncertainties in both the analytical and thermodynamic data used.

For thermobarometric calculations we used the internally consistent thermodynamic dataset of Perchuk *et al.* (1985) and Perchuk (1990), which is calibrated on the basis of experimental data on mineral equilibria involving solid solutions of garnet, orthopyroxene and cordierite (Perchuk & Lavrent'eva, 1983; Aranovich & Podlesskii, 1989). However, the results obtained are not specific to this dataset. Similar conclusions can be reached with the use of other datasets such as that of Holland & Powell (1998), applicable to the calculation of phase diagrams for cordierite-bearing granulites (e.g. Gerya *et al.*, 2001). The procedure followed to derive realistic P–T paths involves the following four major steps [see Perchuk *et al.* (1996, 2000*b*) and Smit *et al.* (2001), for further elaboration as well as details on calculations and worked examples].

(1) The sequence of events responsible for the formation of minerals and observed reaction textures is established.

(2) The chemical evolution of rock-forming minerals is determined by detailed microprobe profiling, allowing the distinction between exchange (diffusion) and net-transfer (mineral growth/decomposition) reaction mechanisms.

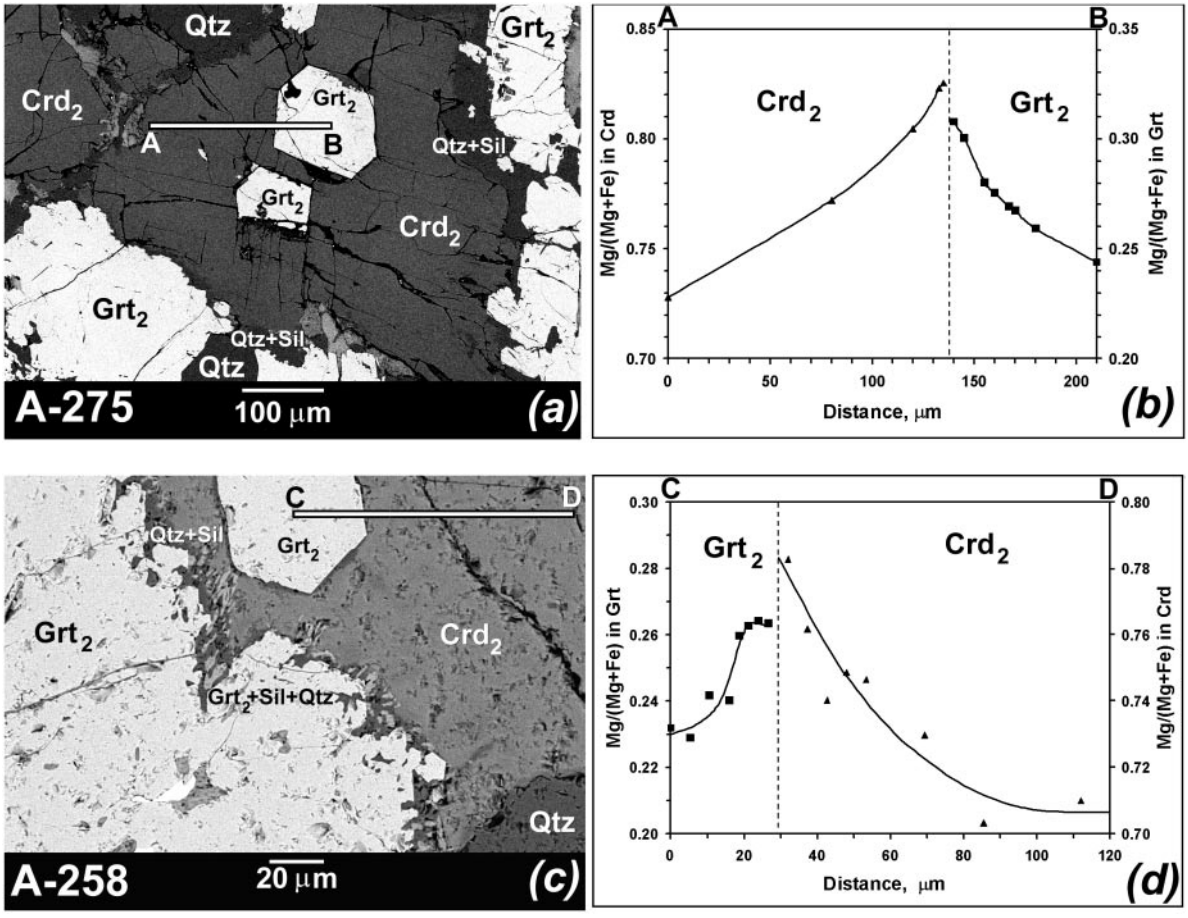

Fig. 6. Back-scattered electron images (a, c) and chemical zoning patterns (b, d) of newly formed idioblastic garnet (Grt_2) in samples studied.

(3) Specific *P–T* coordinates are calculated for the different stages of formation of mineral assemblages using the 'core–core → rim–rim' method for each given generation of minerals. Representative rim compositions are selected on the basis of microprobe profiling to avoid the influence of later exchange diffusion on thermobarometry (e.g. Frost & Chacko, 1989; Spear & Florence, 1992). Equilibrium compositions of cores are assumed for relatively large (>1 mm) mineral grains that show chemical profiles with a central plateau of constant composition (e.g. Spear & Florence, 1992). Temperatures are calculated (Table 3) using garnet–cordierite pairs (Perchuk and Lavrent'eva, 1983) and pressures obtained from garnet–sillimanite–cordierite–quartz (Perchuk *et al.*, 1985, 2000*b*).

(4) A *P–T* trajectory is derived on the basis of individually calculated *P–T* points. The consistency of the *P–T* trajectory is tested with both mineral zoning (i.e. the relationship between the *P–T* path vector and the array of calculated compositional isopleths in observed divariant assemblages) and the observed reaction textures. For the latter, we relate the *P–T* path to isopleths of relative garnet mode in the observed divariant assemblages (Gerya, 1991; Perchuk *et al.*, 2000*b*; Smit *et al.*, 2001). The isopleths of relative garnet mode, representing the atomic ratio $100(Mg + Fe)_{in\ garnet}/(Mg + Fe)_{in\ rock}$, are calculated by solving a system of thermodynamic and mass balance equations for the observed cordierite + garnet + sillimanite + quartz assemblage on the basis of the bulk-rock compositions given in Table 2 [see Perchuk *et al.* (2000*b*) and Smit *et al.* (2001) for details of the method of calculation]. By comparing the *P–T* path with the isopleths of relative garnet mode it can be inferred whether garnet should grow or decompose along a specific section of this path, a conclusion that can in turn be tested by reaction textures studied in the sample. The calculation of isopleths of relative garnet mode assumes complete re-equilibration of a rock with changing *P–T* parameters, which is not realized in most cases. Therefore the comparison with *P–T* paths obtained by thermobarometry is a qualitative test.

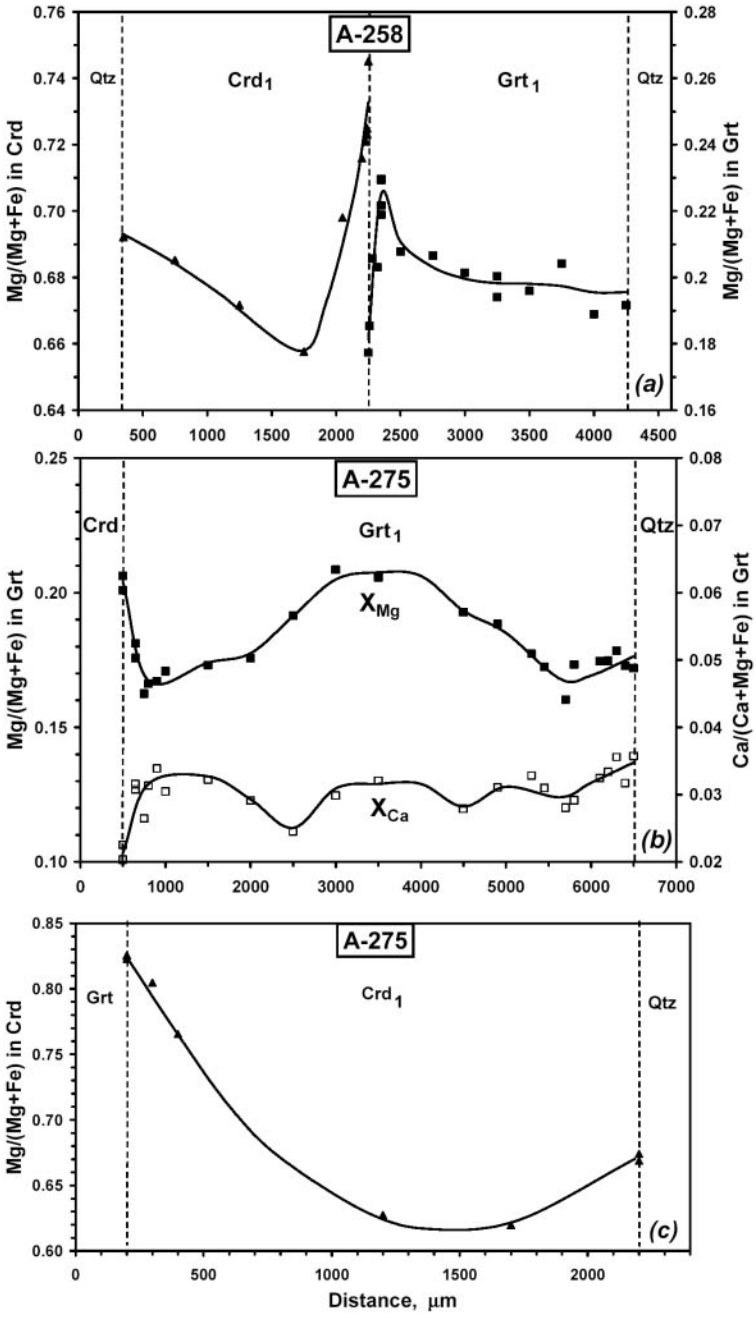

Fig. 7. Typical chemical zoning profiles for contacting porphyroblasts of early garnet (Grt_1) and cordierite (Crd_1) for samples A-258 (a) and A-275 (b), (c) collected ~3 km from the boundary of the Kanskiy complex.

Thermodynamic calculations for the divariant assemblage Grt + Sil + Crd + Qtz were carried out using internally consistent thermodynamic data (Perchuk *et al.*, 1985) for the reactions

$$1/3\text{Prp} + 2/3\text{Sil} + 5/6\text{Qtz} = 1/2\text{Crd-Mg}$$

$$(\Delta H = 51 \text{ cal}, \Delta S = 4{\cdot}620 \text{ cal/K}, \Delta V = 0{\cdot}63827 \text{ cal/bar})$$

and

$$1/3\text{Prp} + 1/2\text{Crd-Fe} = 1/3\text{Alm} + 1/2\text{Crd-Mg}$$

$$(\Delta H = -6134 \text{ cal}, \Delta S = -2{\cdot}668 \text{ cal/K}, \Delta V = -0{\cdot}03535 \text{ cal/bar}).$$

Activities of the solid-solution end-members were calculated as follows (Perchuk *et al.*, 1985; Gerya &

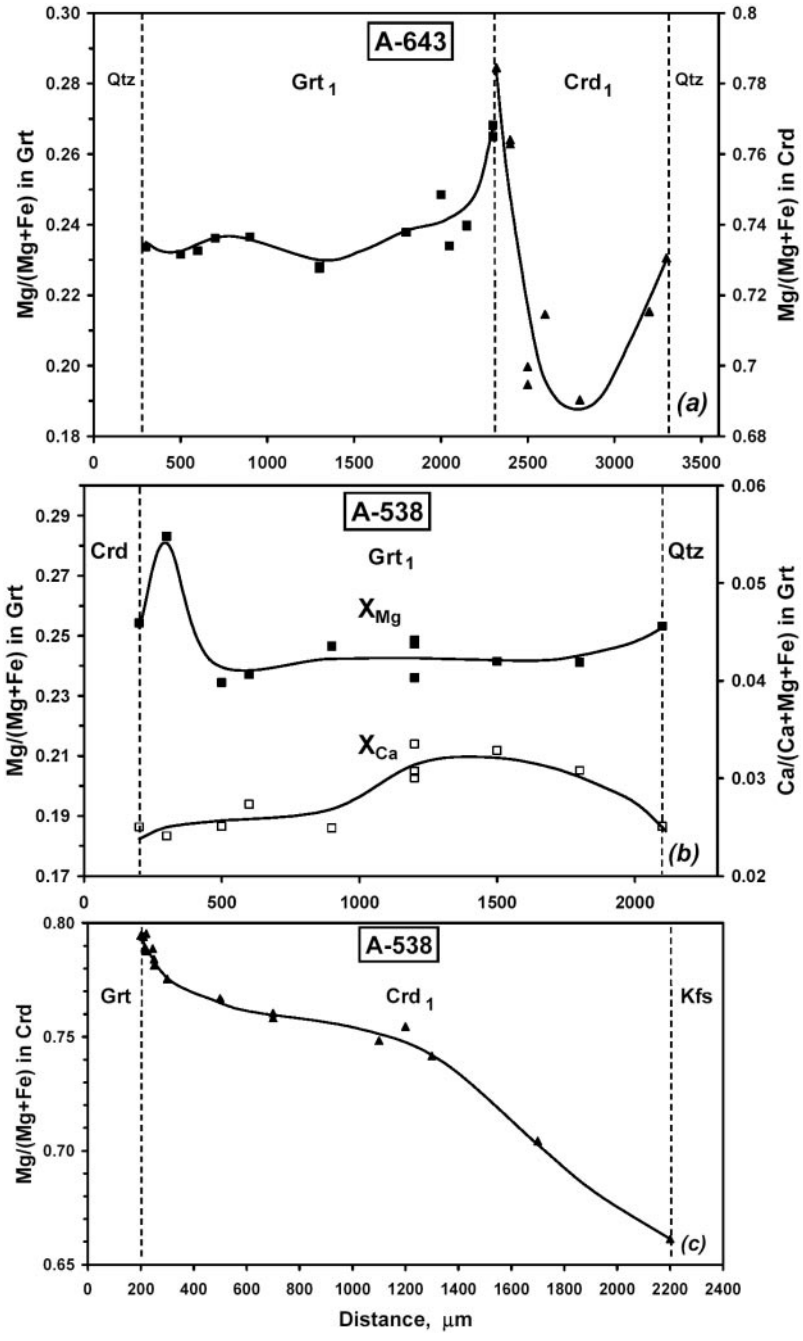

Fig. 8. Typical chemical zoning profiles for contacting porphyroblasts of early garnet (Grt_1) and cordierite (Crd_1) for samples A-643 (a) and A-538 (b, c) collected ~8 km from the boundary of the Kanskiy complex.

Perchuk, 1990):

$$RT \ln a_{Prp}^{Grt} = 3RT \ln X_{Mg}^{Grt}$$

$$RT \ln a_{Alm}^{Grt} = 3RT \ln X_{Fe}^{Grt}$$

$$RT \ln a_{Crd\text{-}Mg} = 2RT \ln X_{Mg}^{Crd} + W$$

$$RT \ln a_{Crd\text{-}Fe} = 2RT \ln X_{Fe}^{Crd} + W$$

where $W = -1333 + 0{\cdot}617T - 0{\cdot}336P + 1026(1 - X_{H_2O}) + 472(1 - X_{H_2O})^2$, $X_{Mg} = Mg/(Fe + Mg)$; $X_{Fe} = Fe/(Fe + Mg)$; $X_{H_2O} = H_2O/(H_2O + CO_2)$ is the mole fraction of water in the metamorphic fluid.

We believe that the systematic application of the above procedure allows the derivation of a *P–T* path that is consistent with both mineral zoning and reaction textures, and, therefore, has a very good chance of closely

Table 3: Selected P–T coordinates of garnet–cordierite–sillimanite–quartz equilibria for samples from Table 1

Grt				Crd			
Spot no.	X_{Mg}	X_{Ca}	X_{Mn}	Spot no.	X_{Mg}	T (°C)	P (kbar)
Sample A-538, Grt_1 + Crd_1							
74-c*	0·232	0·030	0·003	25-c	0·643	742	5·05
75-c	0·233	0·031	0·003	199-c	0·701	662	4·35
90-c	0·241	0·033	0·003	27-c	0·704	671	4·50
98-r	0·249	0·026	0·000	167-r	0·755	612	4·09
105-r	0·262	0·033	0·000	162-r	0·774	603	4·14
Sample A-538, Grt_2 + Crd_2							
102-c	0·260	0·024	0·000	149-c	0·789	579	3·94
106-c	0·276	0·025	0·000	163-c	0·795	591	4·18
94-c	0·283	0·024	0·000	152-c	0·775	630	4·56
78-r	0·248	0·025	0·000	79-r	0·787	566	3·72
126-r	0·248	0·024	0·000	127-r	0·801	547	3·58
Sample A-643, Grt_1 + Crd_1							
P36-c	0·237	0·033	0·011	P44-c	0·690	684	4·58
P51-c	0·234	0·028	0·006	P43-c	0·700	665	4·38
P60-c	0·229	0·030	0·010	P6-c	0·658	714	4·77
Sample A-643, Grt_2 + Crd_2							
P41-r	0·268	0·023	0·006	P42-r	0·784	597	4·15
P49-r	0·265	0·020	0·011	P48-r	0·764	622	4·32
P52-r	0·237	0·023	0·009	P53-r	0·763	584	3·75
Sample A-258, Grt_1 + Crd_1							
2-c	0·201	0·030	0·063	85-c	0·642	684	4·20
3-c	0·207	0·030	0·061	E18-c	0·658	674	4·18
11-r	0·204	0·033	0·059	E17-r	0·672	650	3·94
Sample A-258, Grt_2 + Crd_2							
E22-c	0·252	0·017	0·044	E23-c	0·758	612	4·12
A28-c	0·263	0·018	0·050	A33-c	0·762	622	4·31
E1-r	0·206	0·019	0·054	E4-r	0·721	592	3·47
E2-r	0·177	0·018	0·062	E3-r	0·723	544	2·75
E8-r	0·210	0·014	0·052	E14-r	0·745	569	3·34
Sample A-275, Grt_1 + Crd_1							
P8-c	0·209	0·030	0·012	D6-c	0·578	791	5·29
P9-c	0·206	0·032	0·013	D5-c	0·599	753	4·89
P7-c	0·191	0·025	0·015	D4-c	0·606	711	4·38
32-c	0·205	0·033	0·004	D25-c	0·635	701	4·43
113-r	0·184	0·034	0·010	D21-r	0·627	669	3·88
P5-r	0·173	0·032	0·019	D7-r	0·620	655	3·63
Sample A-275, Grt_2 + Crd_2							
D11-c	0·244	0·030	0·006	D14-c	0·728	642	4·29
P14-c	0·201	0·020	0·007	30-c	0·663	656	3·96
101-r	0·259	0·033	0·011	D13-r	0·772	602	4·10
103-r	0·308	0·015	0·005	108-r	0·823	586	4·43
105-r	0·300	0·013	0·004	109-r	0·825	573	4·26

Grt Spot no.	X_{Mg}	X_{Ca}	X_{Mn}	Crd Spot no.	X_{Mg}	*T* (°C)	*P* (kbar)
106-r	0·280	0·020	0·004	110-r	0·805	580	4·14
D19-r	0·258	0·017	0·000	D20-r	0·765	610	4·16
120-r	0·193	0·025	0·012	119-r	0·729	562	3·09
D30-r	0·183	0·026	0·012	D28-r	0·723	554	2·90

*c, core; r, rim.
X_{Mg} = Mg/(Mg + Fe), X_{Ca} = Ca/(Ca + Mg + Fe), X_{Mn} = Mn/(Mn + Ca + Mg + Fe). Temperatures calculated using experimentally calibrated garnet–cordierite geothermometer (Perchuk & Lavrent'eva, 1983) at pressures estimated with the garnet–sillimanite–cordierite–quartz geobarometer (Perchuk, *et al.*, 1985, 2000*b*) with activity of cordierite calculated at X_{H_2O}= 0·2 in coexisting metamorphic fluid (see Table 4).

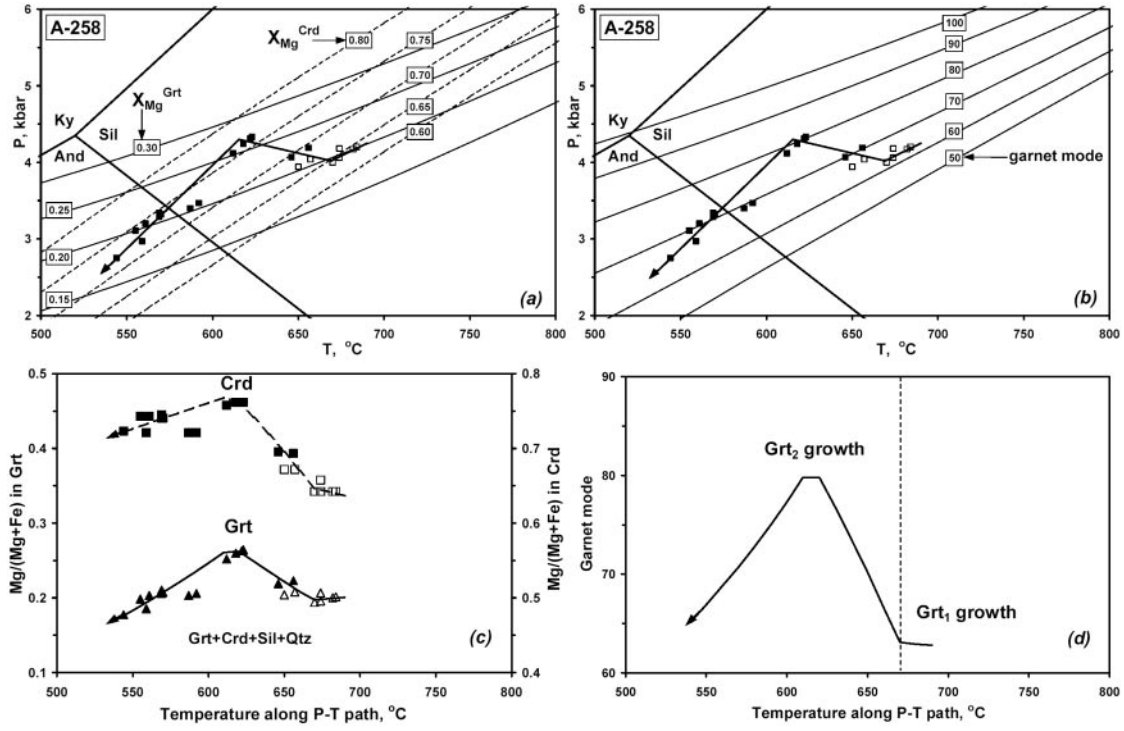

Fig. 9. The *P–T* path (continuous black line) derived for the metamorphic evolution of sample A-258 (locality 1 in Fig. 1). □, *P–T* data for the early generation of garnet (Grt_1); ■, *P–T* data for the later generation (Grt_2). (a) *P–T* path and compositional isopleths for the garnet + sillimanite + cordierite + quartz assemblage. (b) Relationship of *P–T* path to isopleths of garnet mode [atomic ratio $100(Mg + Fe)_{in\ garnet}/(Mg + Fe)_{in\ rock}$]. (c) Calculated equilibrium compositions of minerals along the derived *P–T* path. (d) Calculated equilibrium relative garnet modes along the derived *P–T* path.

approximating the actual *P–T* trajectory of the rock. The accuracy of individual *P–T* coordinates calculated along this trajectory depends on the uncertainties in both the analytical and thermodynamic data involved. For the present study this accuracy can be estimated to be ±30°C and ±0·5 kbar (Perchuk *et al.*, 1985; Perchuk, 1990). To minimize the influence of the thermodynamic uncertainties on our results we used the same set of geothermometers and geobarometers for all studied samples. This allows accurate relative comparison of the geometry of *P–T* paths inferred for different samples on the basis of different patterns of garnet and cordierite zoning (see Figs 5, 7 and 8).

Results

Figures 9–12 show the results of thermobarometry and *P–T* paths derived from reaction textures and mineral zoning. Selected compositions of coexisting garnet and

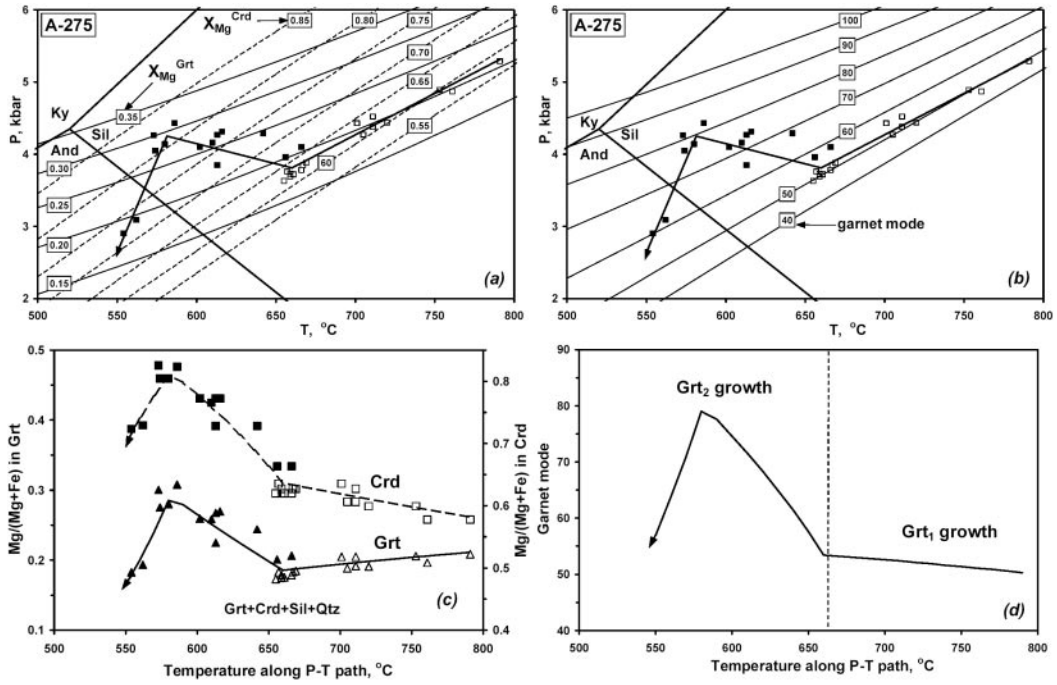

Fig. 10. The *P–T* path (continuous black line) derived for the metamorphic evolution of sample A-275 (locality 1 in Fig. 1). □, *P–T* data for the early generation of garnet (Grt_1); ■, *P–T* data for the later generation (Grt_2). (a) *P–T* path and compositional isopleths for the garnet + sillimanite + cordierite + quartz assemblage. (b) Relationships of *P–T* path with isopleths of relative garnet mode [atomic ratio $100(Mg + Fe)_{in\ garnet}/(Mg + Fe)_{in\ rock}$]. (c) Calculated equilibrium compositions of minerals along the derived *P–T* path. (d) Calculated equilibrium relative garnet modes along the derived *P–T* path.

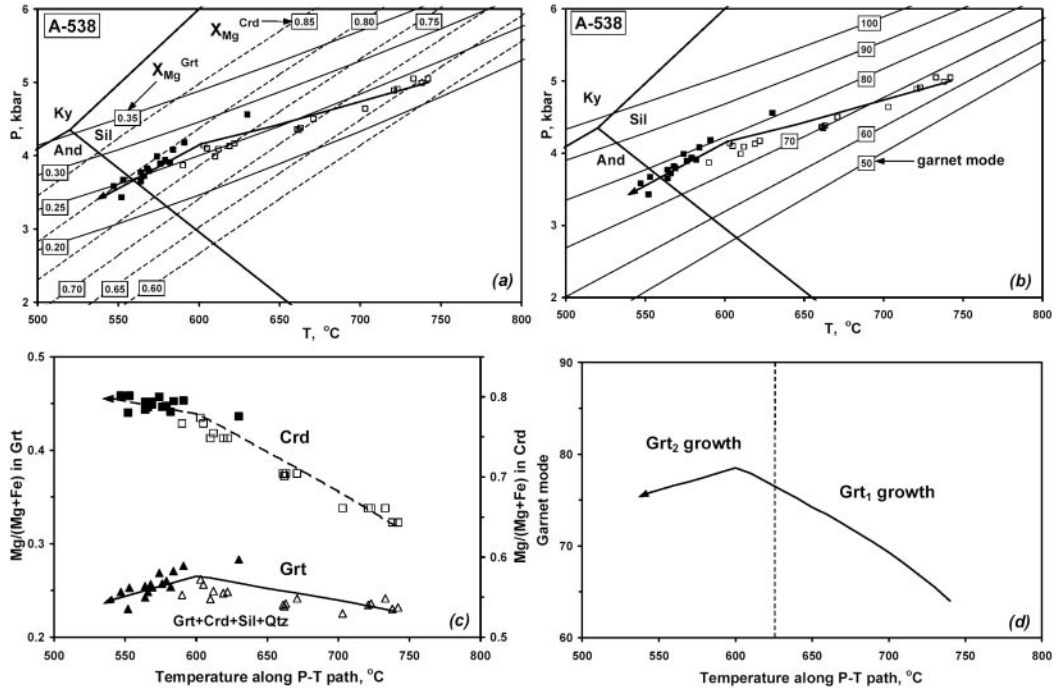

Fig. 11. The *P–T* path (continuous black line) derived for the metamorphic evolution of sample A-538 (locality 2 in Fig. 1). □, *P–T* data for the early generation of garnet (Grt_1); ■, *P–T* data for the later generation (Grt_2). (a) *P–T* path and compositional isopleths for the garnet + sillimanite + cordierite + quartz assemblage. (b) Relationships of *P–T* path with isopleths of relative garnet mode [atomic ratio $100(Mg + Fe)_{in\ garnet}/(Mg + Fe)]_{in\ rock}$]. (c) Calculated equilibrium compositions of minerals along the derived *P–T* path. (d) Calculated equilibrium relative garnet modes along the derived *P–T* path.

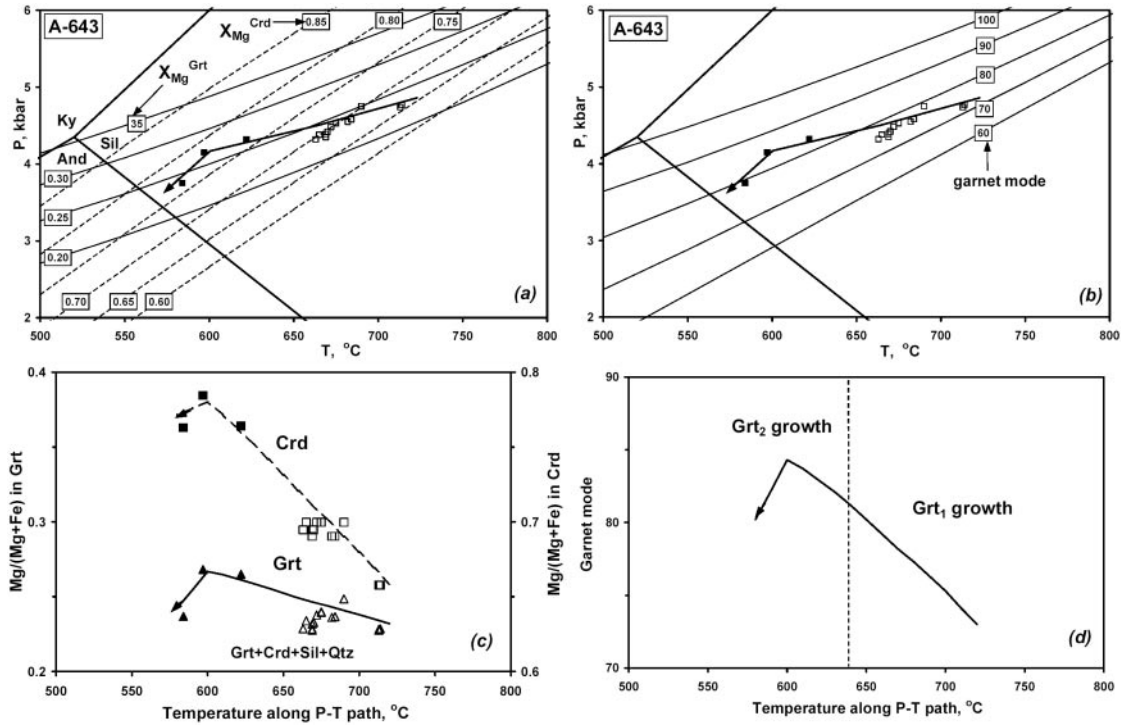

Fig. 12. The *P–T* path (continuous black line) derived for the metamorphic evolution of sample A-643 (locality 2 in Fig. 1). □, *P–T* data for the early generation of garnet (Grt_1); ■, *P–T* data for the later generation (Grt_2). (a) *P–T* path and compositional isopleths for the garnet + sillimanite + cordierite + quartz assemblage. (b) Relationships of *P–T* path with isopleths of relative garnet mode [atomic ratio $100(Mg + Fe)_{in\ garnet}/(Mg + Fe)_{in\ rock}$]. (c) Calculated equilibrium compositions of minerals along the derived *P–T* path. (d) Calculated equilibrium relative garnet modes along the derived *P–T* path.

cordierite and the resulting *P–T* estimates are listed in Table 3. The *P–T* paths for samples from the two studied localities are distinctly different. For samples collected far from the boundary of the Kanskiy complex (locality 2), essentially linear, near-isobaric cooling *P–T* trajectories ($dP/dT = 0{\cdot}005$–$0{\cdot}006$ kbar/°C) are characteristic. On the other hand, samples collected close to this boundary demonstrate kinked *P–T* paths with an intermediate interval of burial cooling (i.e. cooling at increasing pressure) with negative dP/dT slope ($-0{\cdot}005$ to $-0{\cdot}006$ kbar/°C). Figures 9c–12c show the results of thermodynamic modelling of X_{Mg} of garnet and cordierite coexisting along the *P–T* paths. These results are consistent with the observed chemical zoning (compare Figs 6–8 and 9c–12c). Figures 9d–12d represent the equilibrium relative modal amounts of garnet calculated along the *P–T* paths using the bulk compositions of the rocks studied (Table 2). As can be seen, an intensive growth of newly formed garnet and garnet–sillimanite–quartz intergrowths replacing cordierite is consistent with conditions of near-isobaric cooling. In particular, the burial cooling stage of samples A-258 and A-275 was associated with a significant increase in the X_{Mg} of growing garnet (Grt_2) reflected by garnet chemical zoning (Fig. 6b and d).

We consider the calculated *P–T* coordinates to be sufficiently accurate and these paths to be real. The authenticity of the *P–T* paths is supported by: (1) consistency of the calculated *P–T* trajectories with both reaction textures and mineral zoning (Figs 9–12); (2) negligible influence of late diffusion (e.g. Frost & Chacko, 1989; Spear & Florence, 1992) on the strong increase in X_{Mg} of garnet toward the contacts with cordierite (Fig. 6b and d). Furthermore, the use of the same geothermobarometric equations for all studied samples suggests that a valid comparison between the *P–T* paths obtained, which is essential for our study, depends on the accuracy of analytical data only. Uncertainties in the thermodynamic data that propagate into uncertainties in the general position and orientation of the *P–T* paths have no major effect on such a relative comparison.

Table 4 contains the compositions of garnet and biotite coexisting with K-feldspar, sillimanite and quartz in the studied samples. Using these compositions, water activity along the *P–T* paths was also estimated (Table 4). All studied samples are characterized by a low water activity (0·15–0·30) that generally decreases with falling temperature. The systematic lowering of water activity after peak metamorphic conditions is consistent with the

Table 4: Selected P–T–a_{H_2O} *parameters of garnet–-biotite–sillimanite–K-feldspar–quartz equilibria for samples from Table 1*

Grt (per 8 oxygens)					*Bt* (per 11 oxygens)										*T* (°C)	*P* (kbar)	a_{H_2O}
Spot no.	Fe	Mn	Mg	Ca	Spot no.	Si	Ti	Al	Fe	Mn	Mg	Ca	Na	K			
Sample A-538, early garnet (Grt_1) and biotite in the matrix																	
89-c*	2·219	0·009	0·686	0·101	19-c	2·734	0·093	1·551	1·178	0·000	1·332	0·000	0·000	1·021	689	4·67	0·301
88-c	2·222	0·016	0·727	0·075	14-c	2·750	0·247	1·425	1·148	0·000	1·220	0·000	0·000	0·999	718	4·85	0·266
Sample A-538, younger garnet (Grt_2) and associating biotite																	
104-c	2·206	0·000	0·750	0·081	135-c	2·710	0·354	1·335	0·945	0·000	1·402	0·000	0·000	1·048	649	4·42	0·190
140-r	2·249	0·000	0·679	0·096	139-r	2·728	0·315	1·380	0·847	0·000	1·506	0·000	0·026	0·956	588	4·00	0·146
Sample A-643, early garnet (Grt_1) and biotite in the matrix																	
P34-c	2·351	0·041	0·713	0·098	P46-c	2·736	0·286	1·316	1·144	0·000	1·332	0·000	0·000	1·012	677	4·55	0·268
P37-r	2·308	0·035	0·680	0·096	P47-r	2·722	0·206	1·385	1·060	0·002	1·496	0·000	0·000	1·016	629	4·27	0·242
Sample A-643, younger garnet (Grt_2) and associating biotite																	
P31-r	2·328	0·035	0·667	0·089	P30-r	2·750	0·283	1·291	0·952	0·000	1·530	0·000	0·000	1·030	598	4·06	0·199
P32-r	2·331	0·031	0·711	0·091	P30-r	2·750	0·283	1·291	0·952	0·000	1·530	0·000	0·000	1·030	610	4·15	0·196
Sample A-258, early garnet (Grt_1) and biotite in the matrix																	
9-c	2·264	0·164	0·537	0·067	70-c	2·713	0·281	1·408	1·274	0·000	1·113	0·000	0·000	1·026	685	4·04	0·341
10-c	2·257	0·184	0·526	0·095	70-c	2·713	0·281	1·408	1·274	0·000	1·113	0·000	0·000	1·026	681	4·07	0·339
Sample A-258, younger garnet (Grt_2) and associating biotite																	
A50-c	2·191	0·074	0·663	0·030	A45-c	2·677	0·185	1·576	0·995	0·000	1·466	0·000	0·000	0·904	626	4·27	0·207
69-r	2·403	0·096	0·559	0·034	68-r	2·754	0·260	1·358	0·980	0·000	1·447	0·000	0·000	1·015	573	3·41	0·226
Sample A-275, early garnet (Grt_1) and biotite in the matrix																	
19-c	2·369	0·025	0·574	0·110	53-c	2·712	0·300	1·416	1·303	0·000	1·039	0·000	0·027	0·992	713	4·50	0·330
D17-r	2·516	0·021	0·547	0·063	D24-r	2·743	0·238	1·373	1·229	0·002	1·249	0·000	0·000	0·994	634	4·13	0·334
Sample A-275, younger garnet (Grt_2) and associating biotite																	
20-r	2·375	0·026	0·602	0·088	42-r	2·674	0·248	1·452	1·076	0·000	1·356	0·000	0·111	0·979	621	4·19	0·240
40-r	2·378	0·033	0·512	0·103	39-r	2·834	0·148	1·312	0·944	0·000	1·589	0·000	0·080	0·991	535	2·34	0·200

*c, core; r, rim.

Temperatures calculated using experimentally calibrated garnet–biotite geothermometer (Perchuk & Lavrent'eva, 1983), pressures estimated at calculated temperatures using *P–T* paths for corresponding samples (Figs 9–13), water activity calculated using garnet–biotite–sillimanite–K-feldspar–quartz equilibrium (Perchuk *et al.*, 1985).

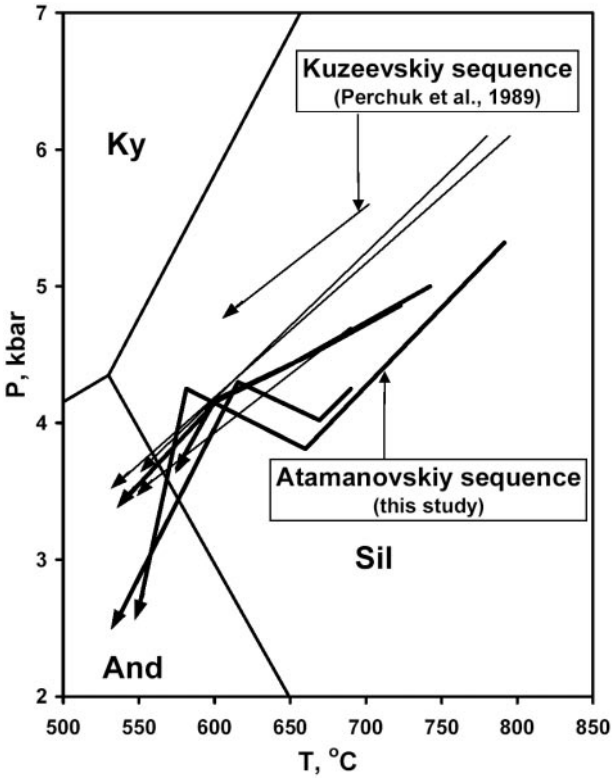

Fig. 13. Summary of *P–T* paths for metapelites of the Kuzeevskiy (Perchuk *et al.*, 1989) and Atamanovskiy (this study) sequences of the Kanskiy granulite complex.

dehydration reaction textures observed in the metapelites (e.g. Fig. 4c).

NUMERICAL MODELLING OF *P–T* PATHS

The metapelites of the Kanskiy granulite complex exhibit characteristic garnet-forming reaction textures and flat *P–T* cooling paths that are consistent with previously published data on this complex (Perchuk *et al.*, 1989). However, an important new result from this study is the distinct difference in the shape of *P–T* paths from different parts of the Kanskiy granulite complex: (1) metapelites collected far (~8 km) from the boundary with the lower-grade Yeniseyskiy complex (e.g. A-538, A-643, Fig. 1) followed a simple, essentially linear near-isobaric cooling path with $dP/dT = 0{\cdot}005$–$0{\cdot}006$ kbar/°C; (2) metapelites collected close (~3 km) to this boundary (e.g. A-258, A-275, Fig. 1) reveal a kinked *P–T* path with an intermediate interval of burial cooling ($dP/dT = -0{\cdot}005$ to $-0{\cdot}006$ kbar/°C). The difference in the shape of the *P–T* paths is supported by reversals in garnet zoning in the second group of samples (e.g. A-275, Fig. 7b).

The diversity of *P–T* paths in the granulites from the Kanskiy granulite complex (Fig. 13) is not unique. As indicated in Fig. 2, similar features have been found in other high-grade terrains such as the Limpopo granulite complex in South Africa (Perchuk *et al.*, 1996, 2000*b*; Smit *et al.*, 2001), the Lapland complex in the Kola Peninsula (Perchuk *et al.*, 1999, 2000*b*), and the Sharizhalgay complex in the Baikal area, Eastern Siberia (Perchuk, 1989). This underscores the general importance of the phenomenon and suggests a systematic genetic pattern indicative of a specific geodynamic process.

The existence of kinked *P–T* paths for metapelites of the Limpopo high-grade terrain (Fig. 2) was first described by Perchuk *et al.* (1996, 2000*b*), who noted that kinked *P–T* paths with low dP/dT cooling portions are characteristic of samples collected close (<45 km) to the boundary of the complex with the Kaapvaal Craton. Perchuk *et al.* (1996, 2000*b*) explained the existence of these two types of *P–T* paths by differences in the relative movement of different crustal blocks during their exhumation. The crustal blocks from central portions of the granulite complex were subjected to straightforward exhumation, allowing their adjustment to the ambient thermal gradient. On the other hand, the *P–T* evolution of ascending blocks close to the boundary of the complex was disturbed at crustal levels of about 13–15 km, where rapid cooling was initiated because of the temperature gradient between the hot granulites and the cooler overridden cratonic rocks.

A physical test of these ideas has been provided by numerical geodynamic experiments (Gerya *et al.*, 2000) based on the gravitational redistribution mechanism suggested by Perchuk (1989) and Perchuk *et al.* (1992) for the exhumation of granulites. Taking into account the inherent gravitational instability (Gerya *et al.*, 2001, 2002) of hot continental crust subjected to the regional low- to medium-pressure granulite-facies conditions characteristic for the Kanskiy complex (Fig. 13), the presence of large amounts of low-density, syn- to late-tectonic granitic rocks within the complex, and thrusting of the granulites of the Kanskiy complex over the lower-grade rocks of the Yeniseyskiy and Yukseevskiy complexes (Smit *et al.*, 2000), the gravitational redistribution (diapiric) model could also be applicable to the studied region.

Figure 14 presents the results of numerical modelling of the buoyant exhumation of a granulite complex scaled to represent the Kanskiy complex from middle crustal depths along the weak tectonic zone formed at a boundary between two cratons (Gerya *et al.*, 2000). This model suggests thrusting of hotter and less dense granulite onto the colder and more dense middle- and upper-crustal complexes. High (10^2) viscosity contrast between weaker granulites and stronger lower-grade rocks results in the intensely complicated internal deformation of the granulite complex associated with the moderate localized planar deformation of the lower-grade complexes.

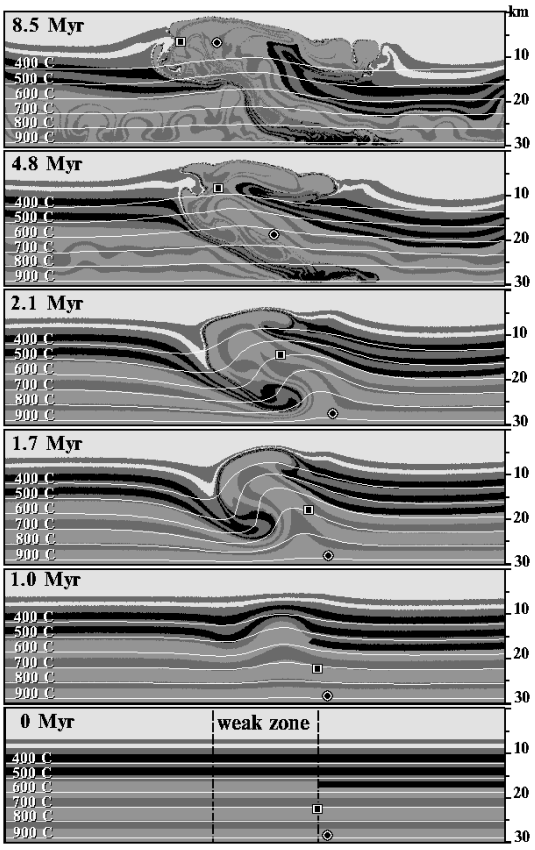

Fig. 14. Results of numerical modelling (Gerya *et al.*, 2000) of the buoyant exhumation of a granulite complex. Model design: size 100 km × 30 km; grid resolution 100 × 30 nodes, 500 × 150 markers; rock types are sediments (white, $\rho = 2700\,kg/m^3$, $\eta = 10^{19}$ Pa s, where ρ is density and η is viscosity), felsic granulites (light grey, $\rho = 2800\,kg/m^3$, $\eta = 10^{19}$ Pa s), metabasites (dark grey, $\rho = 3000\,kg/m^3$, $h = 10^{19}$ Pa s at $T > 600°C$ in granulite sequence, $\eta = 10^{21}$ Pa s at $T < 600°C$ in greenstone sequence), metakomatiites (black, $\rho = 3300\,kg/m^3$, $\eta = 10^{21}$ Pa s) and weak tectonic zone (dashed, $\eta = 10^{19}$ Pa s for all rock types); heat conductivity of rocks is 4 W/m per K; isobaric heat capacity of rocks is 1100 J/kg per K. Initial conditions: $\partial T/\partial x = 0$, $\partial T/\partial z = 0{\cdot}03$ K/m, where x and z are horizontal and vertical coordinates, respectively. Boundary conditions: top—free slip, $T = 27°C$; bottom—no slip, $T = 927°C$; walls—no slip, $\partial T/\partial x = 0$.

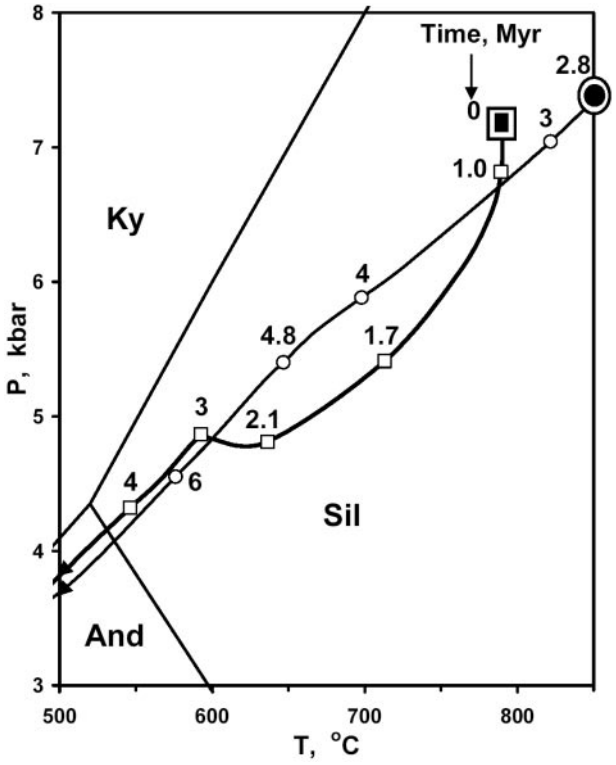

Fig. 15. The results of numerical modelling of *P–T*–time paths for two granulitic fragments shown in Fig. 14. Pressure along the *P–T* paths is calculated as a function of depth neglecting nonlithostatic (e.g. Manktelov, 1995; Petrini & Podladchikov, 2000) component.

An important observation consistent with the petrological data presented here concerns the calculated *P–T* trajectories (Fig. 15) of rock fragments within the exhuming granulite complex (see the two markers in Fig. 14): (1) the fragment exhumed close to the boundary of the complex is characterized by a kinked *P–T* path (see square marker in Figs 14 and 15), whereas (2) the fragment exhumed far from this boundary shows a linear *P–T* trajectory (see round marker in Figs 14 and 15). The numerical modelling suggests (Figs 14 and 15) that the isobaric cooling or even burial cooling intervals of kinked *P–T* paths reflect interaction between an exhuming hot granulite body on the one hand and an overridden cooler cratonic plate on the other. This interaction results in a local convective cell, which causes sub-horizontal movement of granulite towards the cool plate (Fig. 14). This process is typical for the early diapiric uprising stages (0–2 Myr) characterized by significant transient disturbance of the thermal field owing to the rapid (5–10 mm/yr) movement of rocks from different crustal levels (Fig. 14). At the later diapir expansion stages (2–10 Myr), this disturbance vanishes as a result of the decrease in material displacement rates (1–5 mm/yr). Consequently, the rocks exhumed at this latter stage followed simple linear *P–T* trajectories (see round marker in Figs 14 and 15).

This modelled scenario of buoyant exhumation of a granulite complex is also consistent with the results of a recent structural–metamorphic study of the Southern Yenisey Range by Smit *et al.* (2000), which confirms thrusting of the relatively hot and ductile granulites of the Kanskiy complex onto the relatively cold and stiff lower-grade rocks of the Yeniseyskiy and Yukseevskiy complexes. The gravitational redistribution model also predicts the selective accumulation of basic granulites at the tectonic boundary with the overridden lower-grade rocks. This process is related to the differential movement of high-density basic and lower-density felsic rock units within exhuming granulite body (Fig. 14). This prediction

is supported by an increase in the relative amount of metabasites within the Kanskiy complex toward the NW contact with the Yeniseyskiy complex (Nozkhin & Turkina, 1993).

CONCLUSION

The P–T paths derived in this paper for the Kanskiy complex of Eastern Siberia on the basis of thermobarometry and analysis of reaction textures provide another example of contrasting dP/dT development in a granulite complex as a function of distance to the enclosing lower-grade rock sequences. The shapes of the P–T paths found are in accordance with ideas on buoyant exhumation mechanisms for granulites as suggested by Perchuk (1989) and Perchuk *et al.* (1992), as well as numerical and analytical models of Gerya *et al.* (2000, 2001, 2002) for such a process. In a more general sense, we show that such a diversity of P–T paths for a given geodynamic scenario is a logical consequence of the different possible physical trajectories of rocks in a variable thermal field (both in space and time) disturbed by rapid differential movement of material from different crustal levels. Any major geodynamic (i.e. orogenic) process may lead to an array of diverse but interrelated P–T paths recorded by metamorphic rocks (e.g. Willner *et al.*, 2002) from different localities within the complex. Conversely, the nature of this array will provide definitive evidence for the nature of the geodynamic process itself.

ACKNOWLEDGEMENTS

The authors appreciate the help of E. V. Guseva and N. N. Korotaeva during the microprobe study. This work was carried out through the support of RFBR grant 03-05-64633, an Alexander von Humboldt Foundation Research Fellowship to T.V.G. and the Sonderforschungsbereich 526 at Ruhr-University Bochum, funded by the Deutsche Forschungsgemeinschaft. Constructive reviews by Michael Brown and Chris Carson are greatly appreciated.

SUPPLEMENTARY DATA

Supplementary data for this paper are available at *Journal of Petrology* online.

REFERENCES

Aranovich, L. Y. & Podlesskii, K. K. (1989). Geothermobarometry of high-grade metapelites: simultaneously operating reactions. In: Daly, J. S., Yardley, B. W. D. & Cliff, B. R. (eds) *Evolution of Metamorphic Belts. Geological Society, London, Special Publications* **43**, 41–65.

Bibikova, E. V., Gracheva, T. V., Makarov, V. A. & Nozkhin, A. D. (1993). Age boundaries in the geological evolution of Early Precambrian of Yenisey range. *News of Russian Academy of Sciences, Stratigraphy and Geological Correlations* **1**, 35–40 (in Russian).

Dacenko, V. M. (1984). *Granitoid Magmatism of South-western Environment of Siberian Platform*. Novosibirsk: SNIIGGIMS Press (in Russian).

Dacenko, V. M. (1995). *Niznekanskiy Massif—a Standard of Niznekanskiy Granitoid Complex (Yenisey Range)*. Novosibirsk: SNIIGGIMS Press (in Russian).

Frost, B. R. & Chacko, T. (1989). The granulite uncertainty principle: limitations on thermobarometry in granulites. *Journal of Geology* **97**, 435–450.

Gerling, E. K. & Artemov, Yu. M. (1964). Absolute geochronology of south and central parts of the Yenisey range. *Geochemistry* **7**, 610–622 (in Russian).

Gerya, T. V. (1991). Method of physicochemical modeling of metamorphic reactions by using mass-balance condition. *Contributions to Physicochemical Petrology* **16**, 112–127 (in Russian).

Gerya, T. V. & Perchuk, L. L. (1990). GEOPATH—a thermodynamic database for geothermobarometry and related calculations with the IBM PC computer. In: *International Conference 'Metamorphic Styles in Young and Ancient Orogenic Belts'. Program and Abstracts*. Calgary: University of Calgary Press, pp. 59–61.

Gerya, T. V., Dacenko, V. M., Zablotskiy, K. A., Kornev, T. Ya., Lepezin, G. G., Nozkhin, A. D., Popov, N. V., Reverdatto, V. V. & Shvedenkov, G. Yu. (1986). *Precambrian Crystalline Complexes of the Yenisey Range*. Novosibirsk: Institute of Geology and Geophysics Siberian Branch USSR Academy of Sciences Press (in Russian).

Gerya, T. V., Perchuk, L. L., van Reenen, D. D. & Smit, C. A. (2000). Two-dimensional numerical modeling of pressure–temperature–time paths for the exhumation of some granulite facies terrains in the Precambrian. *Journal of Geodynamics* **30**, 17–35.

Gerya, T. V., Maresch, W. V., Willner, A. P., Van Reenen, D. D. & Smit, C. A. (2001). Inherent gravitational instability of thickened continental crust with regionally developed low- to medium-pressure granulite facies metamorphism. *Earth and Planetary Science Letters* **190**, 221–235.

Gerya, T. V., Perchuk, L. L., Maresch, W. V., Willner, A. P., Van Reenen, D. D. & Smit, C. A. (2002). Thermal regime and gravitational instability of multi-layered continental crust: implications for the buoyant exhumation of high-grade metamorphic rocks. *European Journal of Mineralogy* **14**, 687–699.

Harley, S. L. (1989) The origin of granulites: a metamorphic perspective. *Geological Magazine* **126**, 215–231.

Holland, T. J. B. & Powell, R. (1998). Internally consistent thermodynamic data set for phases of petrological interest. *Journal of Metamorphic Geology* **16**, 309–344.

Kovrigina, E. K. (1973). Petrology of metamorphic sequences of Early Precambrian Angaro-Kanskiy part of the Yenisey Range. Ph.D. thesis, VSEGEI, Leningrad (in Russian).

Kovrigina, E. K. (1977). *Tectonics of the Angaro-Kanskiy Part of the Yenisey Range. Reports on Tectonics and Magmatism of Siberia*. Leningrad: VSEGEI Press, pp. 24–40 (in Russian).

Kretz, R. (1983). Symbols for rock-forming minerals. *American Mineralogist* **68**, 277–279.

Kusnetsov, Yu. A. (1941). *Petrology of the Yenisey Range. Data on Geology of Western Siberia*. Tomsk: ZSGU Press (in Russian).

Kusnetsov, Yu. A. (1988). *Selected Works. V. I. Petrology of the Precambrian of the Southern Yenisey Range*. Novosibirsk: Nauka (in Russian).

Manktelov, N. S. (1995). Nonlithostatic pressure during sediment subduction and the development and exhumation of high pressure metamorphic rocks. *Journal of Geophysical Research* **100**, 571–583.

Mints, M. V., Glaznev, V. N., Konilov, A. N., Kunina, N. M., Nikitichev, A. P., Raevsky, A. B., Sedikh, Yu. N., Stupak, V. M. & Fonarev, V. I. (1996). *The Early Precambrian of the North-Eastern Baltic*

Shield: Paleogynamics, Crustal Structure, and Evolution. Moscow: Scientific World Press (in Russian).

Newton, R. C. (1995). Simple-system mineral reactions and high-grade metamorphic fluids. *European Journal of Mineralogy* **7**, 861–881.

Nozkhin, A. D. (1983). Early Precambrian gneiss complexes of the Yenisey Range and their geochemical features. *Geology and Geophysics* **9**, 3–11 (in Russian).

Nozkhin, A.D. (1985). Early Precambrian trough complexes of the south-western part of the Siberian platform and its metallogeny. In: *Precambrian Trough Structures of the Baykal–Amur Region and its Metallogeny*. Novosibirsk: Nauka, pp. 34–46 (in Russian).

Nozkhin, A. D. (1997). Petrogeochemical typization of Precambrian complexes of the south of Siberia. D.Sc. thesis, Institute of Geology, Geophysics and Mineralogy Siberian Branch Russian Academy of Sciences Press, Novosibirsk (in Russian).

Nozkhin, A. D. & Turkina, O. M. (1993). *Geochemistry of Granulites*. Novosibirsk: Institute of Geology and Geophysics Russian Academy of Sciences Press (in Russian).

Nozkhin, A. D., Malishev, V. I., Sumin, A. V., Ostapenko, E. I. & Gerya, T.V. (1989). Age of metamorphic complexes in south-western part of Siberian platform after the data of Pb-isotopic studies. *Geology and Geophysics* **1**, 13–22 (in Russian).

Perchuk, L. L. (1989). *P–T*–fluid regimes of metamorphism and related magmatism with specific reference to the Baikal Lake granulites. In: Daly, J. S., Yardley, B. W. D. & Cliff, B. R. (eds) *Evolution of Metamorphic Belts*. *Geological Society, London, Special Publications* **43**, 275–291.

Perchuk, L. L. (1990). Derivation of thermodynamically consistent system of geothermometers and geobarometers for metamorphic and magmatic rocks. In: Perchuk, L. L. (ed.) *Progress in Metamorphic and Magmatic Petrology*. Cambridge: Cambridge University Press, pp. 93–112.

Perchuk, L. L. & Gerya, T. V. (1992). The fluid regime of metamorphism and the charnockite reaction in granulites: a review. *International Geology Review* **34**, 1–58.

Perchuk, L. L. & Gerya, T. V. (1993). Fluid control of charnockitization. *Chemical Geology* **108**, 175–186.

Perchuk, L. L. & Krotov, A. V. (1998). Petrology of the mica schists of the Tanaelv belt in the southern tectonic framing of the Lapland granulite complex. *Petrology* **6**, 149–179.

Perchuk, L. L. & Lavrent'eva, I. V. (1983). Experimental investigation of exchange equilibria in the system cordierite–garnet–biotite. *Advances in Physical Geochemistry, 3*. New York: Springer, pp. 199–239.

Perchuk, L. L., Aranovich, L. Ya., Podlesskii, K. K., *et al.* (1985). Precambrian granulites of the Aldan shield, eastern Siberia, USSR. *Journal of Metamorphic Geology* **3**, 265–310.

Perchuk, L. L., Gerya, T. V. & Nozhkin, A. D. (1989). Petrology and retrogression in granulites of the Kanskiy Formation, Yenisey Range, Eastern Siberia. *Journal of Metamorphic Geology* **7**, 599–617.

Perchuk, L. L., Podladchikov, Yu. Yu. & Polyakov, A. N. (1992). Geodynamic modeling of some metamorphic processes. *Journal of Metamorphic Geology* **10**, 311–318.

Perchuk, L. L., Gerya, T. V. & Korsman, K. (1994). A model for charnockitization of gneissic complexes. *Petrology* **2**, 395–423.

Perchuk, L. L., Gerya, T. V., van Reenen, D. D., Safonov, O. G. & Smit, C. A. (1996). The Limpopo metamorphic complex, South Africa: 2. Decompression/cooling regimes of granulites and adjusted rocks of the Kaapvaal craton. *Petrology* **4**, 571–599.

Perchuk, L. L., Krotov, A. V. & Gerya, T. V. (1999). Petrology of amphibolites of the Tanaelv Belt and granulites of the Lapland complex. *Petrology* **7**, 339–363.

Perchuk, L. L., Gerya, T. V., Van Reenen, D. D., Smit, C. A. & Krotov, A. V. (2000*a*). *P–T* paths and tectonic evolution of shear zones separating high-grade terrains from cratons: examples from Kola Peninsula (Russia) and Limpopo Region (South Africa). *Mineralogy and Petrology* **69**, 109–142.

Perchuk, L. L., Gerya, T. V., van Reenen, D. D., Krotov, A. V., Safonov, O. G., Smit, C. A. & Shur, M. Yu. (2000*b*). Comparative petrology and metamorphic evolution of the Limpopo (South Africa) and Lapland (Fennoscandia) high-grade terrains. *Mineralogy and Petrology* **69**, 69–107.

Perchuk, L. L., Safonov, O. G., Gerya, T. V., Fu, B. & Harlov, D. E. (2000*c*). Mobility of components in metasomatic transformation and partial melting of gneisses: an example from Sri Lanka. *Contributions to Mineralogy and Petrology* **143**, 673–693.

Petrini, K. & Podladchikov, Yu. (2000). Lithospheric pressure–depth relationship in compressive regions of thickened crust. *Journal of Metamorphic Geology* **18**, 67–77.

Pozhilenko, V. I., Smolkin, V. F. & Sharov, N. V. (1997). Seismic–geological models for the Earth's crust in the Lapland–Pechenga region, Russia. In: Sharov, N. V. (ed.) *A Seismological Model of the Lithosphere of Northern Europe: Lapland–Pechenga Region*. Apatity: Kola Scientific Center, Russian Academy of Sciences, pp. 181–208 (in Russian).

Roering, C., Van Reenen, D. D., Smit, C. A., Barton, J. M., Jr, de Beer, J. H., de Wit, M. J., Stettler, E. H., Van Schalkwyk, J. F., Stevens, G. & Pretorius, S. (1992*a*). Tectonic model for the evolution of the Limpopo Belt. *Precambrian Research* **55**, 539–552.

Roering, C., Van Reenen, D. D., de Wit, M. J., Smit., C. A., de Beer, J. H. & Van Schalkwyk, J. F. (1992*b*). Structural geological and metamorphic significance of the Kaapvaal Craton–Limpopo Belt contact. *Precambrian Research* **55**, 69–80.

Serenko, V. P. (1969). New data on metamorphism of the southern part of the Yenisey Range. *Geology and Geophysics* **9**, 136–141 (in Russian).

Smit, C. A., Van Reenen, D. D., Gerya, T. V., Varlamov, D. A & Fed'kin, A. V. (2000). Structural–metamorphic evolution of the Southern Yenisey Range of Eastern Siberia: implications for the emplacement of the Kanskiy granulite complex. *Mineralogy and Petrology* **69**, 35–67.

Smit, C. A., Van Reenen, D. D., Gerya, T. V. & Perchuk, L. L. (2001). *P–T* conditions of decompression of the Limpopo high-grade terrain: record from shear zones. *Journal of Metamorphic Geology* **19**, 249–268.

Spear, F. S. (1993). *Metamorphic Phase Equilibria and Pressure–Temperature–Time Paths*. Washington, DC: Mineralogical Society of America.

Spear, F. S. & Florence, F. P. (1992). Thermobarometry in granulites: pitfalls and new approaches. *Precambrian Research* **55**, 209–241.

Van Reenen, D. D., Roering, C., Brandl, G., Smit, C. A. & Barton, J. M., Jr (1990). The granulite facies rocks of the Limpopo belt, southern Africa. In: Vielzeuf, D. & Vidal, Ph. (eds) *Granulites and Crustal Evolution*. Dordrecht: Kluwer, pp. 257–289.

Volobuev, M. I., Zikov, S. I. & Stupnikova, N. I. (1976). Geochronology of Precambrian formations of the Sayan–Yenisey region of Siberia. In: *Actual Questions of Modern Geochronology*. Moscow: Nauka, pp. 96–123 (in Russian).

Volobuev, M. I., Zikov, S. I., Stupnikova, N. I. & Vorob'ev, I. V. (1980). Pb-isotopic geochronology of Precambrian metamorphic complexes of south-western boundary of Siberian platform. In: *Geochronology of Eastern Siberia and Far East*. Moscow: Nauka, pp. 14–30 (in Russian).

Willner, A. P., Sebazungu, E., Gerya, T. V., Maresch, W. V. & Krohe, A. (2002). Numerical modeling of *PT*-paths related to rapid exhumation of high-pressure rocks from the crustal root in the Variscan Erzgebirge Dome (Saxony/Germany). *Journal of Geodynamics* **33**, 281–314.